NIH Public Access
Author Manuscript
Nature. Author manuscript; available in PMC 2015 July 17.

Published in final edited form as:
Nature. 2014 July 17; 511(7509): 353–357. doi:10.1038/nature13426.

ABCB5 is a limbal stem cell gene required for corneal development and repair

Bruce R. Ksander[1,*], **Paraskevi E. Kolovou**[1,*], **Brian J. Wilson**[2,3,4], **Karim R. Saab**[2,3], **Qin Guo**[2,3,4], **Jie Ma**[2,3], **Sean P. McGuire**[1], **Meredith S. Gregory**[1], **William J. B. Vincent**[1], **Victor L. Perez**[5], **Fernando Cruz-Guilloty**[5], **Winston W. Y. Kao**[6], **Mindy K. Call**[6], **Budd A. Tucker**[7], **Qian Zhan**[8], **George F. Murphy**[8], **Kira L. Lathrop**[9], **Clemens Alt**[10], **Luke J. Mortensen**[10], **Charles P. Lin**[10], **James D. Zieske**[1], **Markus H. Frank**[2,3,11,*], and **Natasha Y. Frank**[2,4,11,12,*]

[1]Department of Ophthalmology, Schepens Eye Research Institute, Massachusetts Eye & Ear Infirmary and Harvard Medical School, Boston, Massachusetts 02114, USA

[2]Transplant Research Program, Division of Nephrology, Boston Children's Hospital, Boston, Massachusetts 02115, USA

[3]Departmentof Dermatology, Brigham and Women's Hospital, Boston, Massachusetts 02115, USA

[4]Department of Medicine, VA Boston Healthcare System, Boston, Massachusetts 02130, USA

[5]Bascom Palmer Eye Institute and the Department of Ophthalmology, University of Miami Miller School of Medicine, Miami, Florida 33136, USA

[6]Department of Ophthalmology, University of Cincinnati Medical Center, Cincinnati, Ohio 45229, USA

[7]Stephen A Wynn Institute for Vision Research, Carver College of Medicine, Department of Ophthalmology and Visual Sciences, University of Iowa, Iowa City, Iowa 52242, USA

[8]Department of Pathology, Brigham and Women's Hospital, Boston, Massachusetts 02115, USA

[9]Department of Ophthalmology, University of Pittsburgh School of Medicine & Department of Bioengineering, University of Pittsburgh Swanson School of Engineering, Pittsburgh, Pennsylvania 15213, USA

© 2014 Macmillan Publishers Limited. All rights reserved

Correspondence and requests for materials should be addressed to: N.Y.F. (nfrank@partners.org) or M.H.F. (markus.frank@childrens.harvard.edu).
*These authors contributed equally to this work.

Supplementary Information is available in the online version of the paper.

Author Contributions N.Y.F., M.H.F. and B.R.K. designed the study. P.E.K., B.R.K., N.Y.F., M.H.F., B.J.W., K.R.S., Q.G., J.M., S.P.M., M.S.G., W.J.B.V., Q.Z., K.L.L., C.P.L., C.A. and L.J.M. performed experiments. V.L.P., F.C.-G. and B.A.T. provided reagents and specimens. W.W.Y.K. and M.K.C. provided technical assistance. P.E.K., B.J.W., Q.G., J.M., S.P.M., M.S.G., W.J.B.V., J.D.Z., G.F.M., B.R.K., M.H.F. and N.Y.F. analysed the data. N.Y.F., M.H.F. and B.R.K. wrote the manuscript. M.H.F. and N.Y.F. are co-senior investigators.

The murine *Abcb5* messenger RNA sequence has been deposited in GenBank under accession number JQ655148.

Reprints and permissions information is available at www.nature.com/reprints.

The authors declare competing financial interests: details are available in the online version of the paper.

Readers are welcome to comment on the online version of the paper.

NIH-PA Author Manuscript
NIH-PA Author Manuscript
NIH-PA Author Manuscript

NIH-PA Author Manuscript

NIH-PA Author Manuscript

NIH-PA Author Manuscript

[10]Center for Systems Biology and Wellman Center for Photomedicine, Massachusetts General Hospital and Harvard Medical School, Boston, Massachusetts 02114, USA

[11]Harvard Stem Cell Institute, Harvard Medical School, Boston, Massachusetts 02138, USA

[12]Division of Genetics, Brigham and Women's Hospital, Boston, Massachusetts 02115, USA

Abstract

Corneal epithelial homeostasis and regeneration are sustained by limbal stem cells (LSCs)[1–3], and LSC deficiency is a major cause of blindness worldwide[4]. Transplantation is often the only therapeutic option available to patients with LSC deficiency. However, while transplant success depends foremost on LSC frequency within grafts[5], a gene allowing for prospective LSC enrichment has not been identified so far[5]. Here we show that ATP-binding cassette, sub-family B, member 5 (ABCB5)[6,7] marks LSCs and is required for LSC maintenance, corneal development and repair. Furthermore, we demonstrate that prospectively isolated human or murine ABCB5-positive LSCs possess the exclusive capacity to fully restore the cornea upon grafting to LSC-deficient mice in xenogeneic or syngeneic transplantation models. ABCB5 is preferentially expressed on label-retaining LSCs[2] in mice and p63α-positive LSCs[8] in humans. Consistent with these findings, ABCB5-positive LSC frequency is reduced in LSC-deficient patients. Abcb5 loss of function in *Abcb5* knockout mice causes depletion of quiescent LSCs due to enhanced proliferation and apoptosis, and results in defective corneal differentiation and wound healing. Our results from gene knockout studies, LSC tracing and transplantation models, as well as phenotypic and functional analyses of human biopsy specimens, provide converging lines of evidence that ABCB5 identifies mammalian LSCs. Identification and prospective isolation of molecularly defined LSCs with essential functions in corneal development and repair has important implications for the treatment of corneal disease, particularly corneal blindness due to LSC deficiency.

ABCB5, first identified as a marker of skin progenitor cells[6] and melanoma stem cells[7,9], functions as a regulator of cellular differentiation[6]. On the basis of this function and its expression on stem cells in additional organ systems[10], we hypothesized that ABCB5 might also identify slow-cycling, label-retaining LSCs in the eye. We performed bromodeoxyuridine (BrdU)-based 'pulse-chase' experiments (Extended Data Fig. 1a) in Abcb5 wild-type mice, which revealed 8-week label-retaining cells only in the limbus, but not central cornea (Fig. 1a, b and Extended Data Fig. 1b). BrdU-retaining LSCs were located in basal limbal epithelium and demonstrated Abcb5 co-expression (Fig. 1c, Extended Data Fig. 6c and Supplementary Videos 1 and 2). Abcb5$^+$ cells (range 0.4–2.3%) were predominantly BrdU-positive (75.7 ± 7.5%), in contrast to Abcb5$^-$ cells (3.3 ± 2.3%, $P < 0.001$) (Fig. 1d). Similar to findings in mice (Figs 1c, 2d, e and Extended Data Fig. 3a, b), human ABCB5$^+$ cells were also located in basal limbal epithelium (Fig. 1e). Moreover, they localized to the palisades of Vogt (Fig. 1e, Extended Data Fig. 1c–j and Supplementary Video 3). ABCB5$^+$ limbal cells exclusively contained ΔNp63α$^+$ human LSCs, determined using distinct ΔNp63α antibodies (ΔNp63α/TAp63α epitope positivity in ABCB5$^+$ versus ABCB5$^-$ cells: 28.9 ± 5.7% versus 0.1 ± 0.1%; ΔNp63α,β,γ epitope positivity: 28.9 ± 14.7% versus 0.1 ± 0.1%; $P < 0.05$) (Fig. 1f) and did not express the differentiation marker keratin 12 (KRT12) (Fig. 1g). Moreover, limbal biopsies from LSC-deficient (LSCD) patients

NIH-PA Author Manuscript

NIH-PA Author Manuscript

NIH-PA Author Manuscript

exhibited reduced ABCB5$^+$ frequencies compared to controls (2.8 ± 1.6% versus 20.0 ± 2.6%, $P < 0.001$) (Fig. 1h and Extended Data Fig. 2). ABCB5 expression on label-retaining LSCs in mice and p63α$^+$ LSCs in humans, along with reduced ABCB5$^+$ frequency in clinical LSCD, showed that ABCB5 preferentially marks LSCs.

To investigate Abcb5 function in corneal development and regeneration, we generated *Abcb5* knockout mice lacking exon 10 of the murine gene (GenBank accession number JQ655148), which encodes a functionally critical extracellular domain homologous to amino acids 493–508 of human ABCB5 (ref. 6) (GenBank accession number NM_178559) (Fig. 2a, b). Polymerase chain reaction (PCR) analysis confirmed deletion (Fig. 2c). Abcb5 protein loss was demonstrated using an exon-10-encoded epitope-targeted monoclonal antibody (Fig. 2c), an amino-terminus-targeted antibody (Extended Data Fig. 3c), and a specific extracellular-loop-associated peptide-targeted human immunoglobulin (Ig)G1 monoclonal antibody (clone 3B9) (Fig. 2d and Extended Data Fig. 3a). Wild-type tissues only expressed Abcb5 in the limbus but not the cornea (Fig. 2d and Extended Data Fig. 3a), consistent with findings in human tissues. Specificity of this binding pattern was demonstrated by RNA *in situ* hybridization (Fig. 2e and Extended Data Fig. 3b).

Abcb5 knockout mice were indistinguishable by physical examination from wild-type littermates through adulthood and their eyes contained all anterior and posterior segment components (Fig. 2f and Extended Data Fig. 3d). However, histological analysis of mutant versus wild-type corneas demonstrated developmental abnormalities characterized by decreased cellularity of the apical epithelial layer and disorganized basal and wing cell layers (Fig. 2f and Extended Data Fig. 3e). No inflammation was noted (Extended Data Fig. 3f). Reduced epithelial cell numbers in the central cornea but not limbus of knockout versus wild-type mice were confirmed by histological enumeration (cornea: 2,688 ± 399 versus 4,427 ± 346 cells, $P < 0.05$; limbus: 3,015 ± 433 versus 3,629 ± 94 cells, P = not significant) (Fig. 2g) and flow cytometry (Extended Data Fig. 3g). Corneas in knockout mice also exhibited epithelial tight junction defects (Fig. 2h) and increased fragility versus wild-type corneas (brush injury frequency 100% versus 33%, $P < 0.001$) (Extended Data Fig. 4a). Moreover, knockout versus wild-type mice showed reduced limbal and corneal Pax6 and corneal Krt12 expression (limbal Pax6: 0.3 ± 0.3% versus 18.0 ± 4.6%; corneal Pax6: 8.3 ± 4.6% versus 42.0 ± 7.6%; corneal Krt12: 6.5 ± 6.5% versus 47.7 ± 8.2%; $P < 0.05$) (Fig. 2h and Extended Data Fig. 3h), also demonstrating an essential role of Abcb5 in corneal development. Additional ocular abnormalities involved the retina (Extended Data Fig. 5), where *ABCB5* is also expressed[11].

Restoring the corneal epithelium after wounding is a hallmark function of LSCs. To determine whether wound healing requires Abcb5, knockout and wild-type mice received central corneal epithelial debridement injuries (Extended Data Fig. 4b–d). Wound closure rates were not significantly different (Extended Data Fig. 4e); however, knockout mice exhibited abnormal corneal restoration characterized by irregular epithelium with reduced cell numbers (403 ± 30 versus 737 ± 28, $P < 0.001$) (Fig. 2i and Extended Data Fig. 4f), increased cellular proliferation (Ki67 limbus: 54.0 ± 5.0% versus 0.3 ± 0.2%, $P< 0.001$; cornea: 41.0± 14.0% versus 7.5 ± 2.4%, $P < 0.05$) (Fig. 2j), and increased apoptosis (limbus:

NIH-PA Author Manuscript

NIH-PA Author Manuscript

NIH-PA Author Manuscript

41.2 ± 12.8% versus 1.0 ± 0.5%; cornea: 49.0 ± 10.0% versus 0.4 ± 0.3%; $P < 0.001$) (Fig. 2k and Extended Data Fig. 4g).

On the basis of our finding that Abcb5 preferentially identifies label-retaining and p63α$^+$ LSCs, we hypothesized that Abcb5 was required for LSC maintenance. We therefore examined quiescent LSCs in knockout versus wild-type mice, using the BrdU-labelling approach (Extended Data Fig. 1a, b). After a 24 h chase, epithelial cells were equally labelled in knockout versus wild-type specimens (5.7 ± 0.9% versus 7.2 ± 1.0%, P = not significant) (Extended Data Fig. 6b). In contrast, after an 8-week chase, label-retaining LSC frequency was reduced in knockout versus wild-type mice (0.1 ± 0.1% versus 0.9 ± 0.3%, $P < 0.05$) (Extended Data Fig. 6a). Histological examination of limbal epithelium confirmed selective loss of BrdU label-retaining cells in knockout versus wild-type mice (Extended Data Fig. 6c, d and Supplementary Video 2), demonstrating that abrogation of Abcb5 function induces LSC proliferation. Consistent with this result, Ki67 expression was enhanced in knockout versus wild-type tissues (limbus: 24.0 ± 5.0% versus 1.5 ± 1.5%, $P < 0.001$; cornea: 53.0 ± 16.0% versus 11.0 ± 2.1%, $P < 0.05$) (Extended Data Fig. 6e). Because cell cycle withdrawal is a prerequisite for LSC maintenance and hence normal differentiation, these results provided one explanation for the corneal differentiation defect in knockout mice. Moreover, impaired cell cycle withdrawal was associated with enhanced apoptosis, demonstrating a novel anti-apoptotic role of Abcb5. Consistent with this function, ABCB5 monoclonal antibody treatment of p63α-rich human limbal epithelial cells, using blocking concentrations[12], induced apoptosis in 30.9 ± 2.9% of cells versus controls ($P < 0.001$), commensurate with ABCB5 expression levels (Extended Data Fig. 6f, g). Moreover, ABCB5 blockade induced pro-apoptotic p53(S15) and p53(S392) and downregulated anti-apoptotic Bcl2 and Bcl-x (also known as Bcl2l1) (Extended Data Fig. 6h, i). In contrast, non-blocking monoclonal antibodies concentrations employed for cell sorting (2 μg ml^{-1}) maintained viability at >90%.

Clinical studies in LSCD have shown that LSC frequency within grafts is critical for long-term transplant success[5]. To investigate whether ABCB5 represents a marker for prospective LSC enrichment, we examined the cornea-regenerative potential of transplanted murine or human unsegregated, ABCB5$^+$ or ABCB5$^-$ limbal cells in syngeneic or immunodeficient NSG mice with induced LSCD (Extended Data Fig. 7). Recipients of syngeneic murine Abcb5$^-$ grafts or vehicle-only negative controls displayed opaque corneas, epithelial conjunctivalization and absence of differentiated Krt12$^+$ cells (0%, in both cases) when analysed 5 weeks after transplantation, consistent with persistent LSCD (Fig. 3a and Extended Data Fig. 8a, b). Recipients of syngeneic unsegregated grafts displayed partial corneal restoration with differentiated Krt12$^+$ cells in the central cornea (17%, enhanced versus Abcb5$^-$ or vehicle-only treatment, $P < 0.01$), but exhibited persistence of LSCD-characteristic epithelial conjunctivalization (Fig. 3a and Extended Data Fig. 8a, b). In contrast, syngeneic Abcb5$^+$ grafts resulted in the development of clear corneas with normal histology, gave rise to more differentiated Krt12$^+$ cells (47%, increased versus unsegregated or Abcb5$^-$ cell treatment or vehicle-only controls, $P < 0.001$) and prevented epithelial conjunctivalization (Fig. 3a and Extended Data Fig. 8a, b).

NIH-PA Author Manuscript NIH-PA Author Manuscript NIH-PA Author Manuscript

NSG recipients of human ABCB5^{-} grafts or vehicle-only controls also displayed epithelial conjunctivalization and an absence of differentiated KRT12^{+} cells (0%, in both cases) 5 weeks after transplantation (Fig. 3b and Extended Data Fig. 8c). NSG recipients of human unsegregated grafts displayed partial corneal restoration with differentiated KRT12^{+} cells in the central cornea (12%, enhanced versus ABCB5^{-} or vehicle-only treatment, $P < 0.01$), but exhibited persistence of LSCD-characteristic epithelial conjunctivalization (Fig. 3b and Extended Data Fig. 8c). Strikingly, only human ABCB5^{+} grafts, negative for KRT12 before transplantation (Extended Data Fig. 7g), produced clear corneas with normal histology and high numbers of KRT12^{+} cells (31%, increased versus vehicle-only or versus ABCB5^{-} or unsegregated limbal cell treatment, $P < 0.001$) and an absence of LSCD-characteristic epithelial conjunctivalization (Fig. 3b and Extended Data Fig. 8c). To confirm that human donor cells caused corneal restoration, we assayed regenerated corneal tissue by PCR with reverse transcription (RT–PCR) for human-specific β2 microglobulin (β2M), an identifier of all human cells, and human-specific PAX6 and KRT12 as markers of corneal differentiation. Only corneal epithelium of recipients grafted with ABCB5^{+} or unsegregated human limbal cells contained human-specific β2M, PAX6 and KRT12 transcripts, whereas vehicle-only-grafted control eyes that did not exhibit corneal restoration did not, confirming human specificity of the RT–PCR assay (Fig. 3b). Moreover, despite similar viability in ABCB5^{-} compared with unsegregated or ABCB5^{+} cell grafts (Extended Data Fig. 7e, f, h), ABCB5^{-}-grafted eyes were deficient in human-specific β2M, PAX6 or KRT12 expression (Fig. 3b), indicating that engraftment capacity was exclusively contained within the ABCB5^{+} cell population.

To further confirm LSC function of ABCB5^{+} limbal cells, we evaluated their capacity for long-term (>1 year) corneal restoration. LSCD-NSG recipients of human ABCB5^{-} grafts or vehicle-only controls, 13 months after transplantation, continued to display epithelial conjunctivalization, reduced epithelial thickness and increased stromal thickness with an absence of differentiated KRT12^{+} cells (0%, in both cases), consistent with persistent LSCD (Fig. 3c and Extended Data Figs 9, 10). NSG recipients of human unsegregated grafts displayed partial corneal restoration with differentiated KRT12^{+} cells in the central cornea (37%, enhanced versus ABCB5^{-} or vehicle-only treatment, $P < 0.001$), but exhibited persistence of LSCD characterized by lower-than-normal epithelial thickness and higher-than-normal stromal thickness (Fig. 3c and Extended Data Figs 9, 10). In contrast, only purified human ABCB5^{+} grafts produced clear corneas with normal histology in recipient NSG mice, with the presence of a stratified epithelial layer containing high numbers of KRT12^{+} cells (88%, increased versus vehicle-only or versus ABCB5^{-} or unsegregated limbal cell treatment, $P < 0.001$) and the absence of LSCD-characteristic epithelial conjunctivalization, accompanied by restoration of normal epithelial and stromal thickness (Fig. 3c and Extended Data Figs 9, 10) and specific detection of human KRT12^{+} corneal cells (pixel intensity per unit area: 42.3 ± 7.7 versus 4.3 ± 0.7, respectively, $P < 0.01$) (Fig. 3d and Extended Data Fig. 9c).

Our findings that ABCB5^{+} cell frequency is reduced in LSCD, that ABCB5-positivity preferentially characterizes slow-cycling and p63α-positive populations, and that prospectively isolated ABCB5^{+} limbal cells are exclusively capable of reversing LSCD

NIH-PA Author Manuscript

NIH-PA Author Manuscript

NIH-PA Author Manuscript

through long-term corneal regeneration show that ABCB5-positivity defines LSCs. This result is further supported by our demonstration that *Abcb5* knockout mice have impaired LSC-dependent corneal development and wound healing through deficient LSC maintenance due to deregulated anti-apoptotic signals. These results have several important implications. First, successful enrichment of human LSCs has the potential to decisively advance the field of LSCD therapy, because long-term clinical success depends on LSC frequency within grafts[5] and because, thus far, no marker for prospective enrichment of bona fide LSCs defined by long-term corneal restorative capacity has been available[13]. Indeed, our study provides initial proof-of-principle for the hypothesis that prospective LSC enrichment within grafts can markedly enhance LSCD therapeutic success. What makes ABCB5 very useful and unique among LSC genes is its expression on the LSC surface, allowing for monoclonal-antibody-based LSC sorting strategies and enrichment as demonstrated in our study, in contrast to intracellularly expressed p63α and alternative candidate LSC-associated genes that have as of yet not been successfully employed for prospective isolation of human LSCs capable of *in vivo* LSCD reversal. This underscores the promise of ABCB5 as a marker for LSC isolation for clinical transplantation. Second, our study reveals a novel *in vivo* physiological function of ABCB5 in maintaining quiescent LSCs, through ABCB5-dependent regulation of apoptotic signalling pathways. This parallels the known anti-apoptotic function of the ABCB5 homologue ABCB1, shown to be mediated through cross-talk with Bcl-x[14]. Finally, our finding that ABCB5 regulates stem cell maintenance is highly relevant to the study of additional ABCB5-expressing normal stem cell populations in other tissues[6,10] and of slow-cycling ABCB5$^+$ cancer stem cells, in which this role might represent one mechanism of multidrug resistance to cell-cycle-specific agents[10,11,15]. The herein described creation of a novel *Abcb5* gene knockout model represents a critical step towards such studies and to further dissection of *ABCB5* gene function in many relevant normal and cancerous tissues.

METHODS

Animals

Male and female C57BL/6J, NOD.Cg-*Prkdc*^{scid} *Il2rg*^{tm1Wjl}/SzJ (NSG), B6;SJL-Tg(ACTFLPe)9205Dym/J and B6.FVB-Tg(EIIa-cre)C5379Lmgd/J mice were purchased from Jackson Laboratory. *Abcb5* knockout mice were generated as described later. All animals were maintained in accordance with the Institutional Guidelines of the Boston Children's Hospital and the Schepens Eye Research Institute, Harvard Medical School. Four-to-twelve-week-old mice were used for the experiments.

Generation of a germline *Abcb5* knockout mouse

We generated a conditional knockout construct by inserting two *loxP* sites flanking murine *Abcb5* exon 10 (GenBank accession number JQ655148) (Fig. 2a, b). A targeting construct was generated by recombineering[16]. In brief, a neomycin resistance cassette flanked by two *loxP* sites (based on plasmid pL-452) was inserted into the BAC clone RP23-161L22 458 base pairs upstream of exon 10 of the murine *Abcb5* gene (GenBank accession number JQ655148). The targeted region of the BAC clone was retrieved by gap repair into the pL-253 plasmid. The retrieved plasmid contained 6,006 bp upstream of exon 10 (not

NIH-PA Author Manuscript NIH-PA Author Manuscript NIH-PA Author Manuscript

including the inserted neo cassette) and 6,384 bp downstream of exon 10. The neomycin resistance cassette was excised by arabinose induction of Cre recombinase to leave a single *loxP* site upstream of exon 10. A neomycin resistance cassette flanked by two FRT sites and one *loxP* site (based on plasmid pL-451) was inserted 460 bp downstream of exon 10 to complete the targeting construct. The targeting plasmid was verified by DNA sequencing and restriction mapping. The linearized plasmid was transfected into TC1 (129S6/SvEvTac derived) embryonic stem (ES) cells and selected in G418 (Sigma-Aldrich) and Fialuridine (Moravek Biochemicals). Resistant colonies were expanded and screened by long-range PCR to identify targeted clones. The left arm was amplified with 5′-GTTGAGGGGAGCAGCCAGAGCAAGGTGAGAAAGGTG-3′ and 5′-TTAAGGGTTATTGAATATGATCGGAATTGGGCTGCAGGAATT-3′ primers yielding a 6,250 bp PCR product (Fig. 2b). The right arm was amplified with 5′-TGGGGCAGGACAGCAAGGGGGAGGAT-3′ and 5′-CTGGTCCCTCTCCTGTGATCTACACAGGCC-3′ primers yielding a 6,384 bp PCR product (Fig. 2b). Two Abcb5-targeted ES clones were identified. These clones were expanded and injected into C57BL/6 blastocysts that were then transferred to the uterus of pseudopregnant females. High-percentage chimaeric male mice (*Abcb5*$^{neo\text{-}loxP/wt}$) were bred into a C57BL/6 background to obtain germline transmission. Germline transmission of the *Abcb5*$^{neo\text{-}loxP}$ allele was confirmed by PCR analysis of genomic DNA using 5′-GGAAGACAATAGCAGGCATGCTGGG-3′, 5′-GGCTGGGGCAACTGAAAAGTAGCAT-3′, and 5′-TTTCAGCTTCAGTTTATCACAATGTGGGTT-3′ primers designed to amplify the 385 bp targeted allele and the 284 bp wild-type allele. Heterozygous *Abcb5*$^{neo\text{-}loxP}$ mice were then intercrossed with hACTB-FLPe transgenic mice[17] to remove the neomycin resistance cassette. PCR analysis of genomic DNA was performed to confirm removal of the neomycin resistance cassette in the genome of *ABCB5*$^{loxP/wt}$ mice using 5′-ACTTGGTGCGGTGACTCTGAATTTTGC-3′ and 5′-TAGCAACATTTCTGGCATTTTAGGCTG-3′ primers designed to amplify a 494 bp neomycin resistance cassette-deleted allele and a 390 bp wild-type allele. To determine the outcome of a complete loss of ABCB5 function, exon 10 of the murine *Abcb5* gene was deleted by breeding *Abcb5*^{loxP} mice with EIIa-Cre mice, which express Cre recombinase at the zygote stage[18,19] (Fig. 2b). Deletion of the genomic region between the two *loxP* sites was confirmed by PCR analysis of genomic DNA using 5′-GGCTGGGGCAACTGAAAAGTAGCAT-3′, 5′-GCAAATGTGTACTCTGCGCTTATTTAATG-3′ and 5′-TGGTGCAGACTACAGACGTCAGTGG-3′ primers designed to amplify a 322 bp *cre*-deleted allele (null) and a 113 bp wild-type (WT) allele (Fig. 2c). Heterozygous *Abcb5*$^{null/WT}$ mice with the germline deletion of exon 10 were intercrossed to produce homozygous *Abcb5*$^{null/null}$ (*Abcb5* knockout) mutants. Mice were maintained on a 129S6/SvEvTac/C57BL/6 mixed genetic background and littermates were used as controls for experimental analyses.

Western blot analysis and human apoptosis array

Abcb5 wild-type and *Abcb5* knockout cell lysates were immunoblotted using monoclonal ABCB5 antibody 3C2-1D12 (ref. 6) (5.5 μg ml^{-1}), a rabbit polyclonal N-terminus-targeted

NIH-PA Author Manuscript

NIH-PA Author Manuscript

NIH-PA Author Manuscript

ABCB5 antibody (1:100 dilution) (Abgent), or an α-tubulin rabbit polyclonal antibody (1:5,000 dilution) (Abcam). A human apoptosis proteome profiler antibody array (R+D Systems) was used according to the manufacturer's instructions, using 400 μg human limbal epithelial cell lysates prepared from cells treated for 48 h with either blocking concentrations[12] of anti-ABCB5 monoclonal antibody clone 3C2-1D12 (ref. 6) or equivalent concentrations of isotype control monoclonal antibody (clone MOPC31C, Sigma). The pixel densities of array spots were quantified using ImageJ software.

RT–PCR

For detection of human-specific gene transcripts, total RNA was isolated from transplanted murine eyes and non-injured murine or human control corneas using the RNAeasy Plus isolation kit (Qiagen) and then transcribed using the High Fidelity RT kit (Applied Biosystems). PCR was performed using Taq 2X Master Mix (New England Biolabs) and the following gene-specific primers. Human β2-microglobulin (B2M, NM_004048): forward 5′-GTGTCTGGGTT TCATCCATC-3′, reverse 5′-AATGCGGCATCTTCAACCTC-3′; human paired box 6 (PAX6, NM_000280.3): forward 5′-CAGCGCTCTGCCGCCTAT-3′, reverse 5′-CATGACCAACACAGATCAAACATCC-3′; human keratin 12 (KRT12, NM_000223.3): forward 5′-GAAGCCGAGGGCGATTACTG-3′, reverse 5′-GTGCTTGTGATTTGGAGTCTGTCAC-3′; and murine β-actin (Actb, NM_007393): forward 5′-TCCTAGCACCATGAAGATC-3′, reverse 5′-AAACGCAGCTCAGTAACAG-3′.

RNA *in situ* hybridization

Abcb5 RNA probes were prepared as follows. PCR-derived RNA probe templates were synthesized by introducing the T7 promoter into the antisense strand and the SP6 promoter into the sense strand. The primer pair (5′-TAATACGACTCACTATAGGGACCATATGCAATGGCGGTAAAG-3′ and 5′-GATTTAGGTGACACTATAGAGACACTTCAGACTCAACACAG-3′) was used to generate the DNA template for antisense and sense RNA probes spanning 144 bp of murine *Abcb5* complementary DNA containing exon 10 (GenBank accession number JQ655148). RNA probe labelling with digoxigenin (DIG) and *in situ* hybridizations were carried out as described previously[20].

BrdU pulse and chase experiments

Four-week-old *Abcb5* knockout mice and their wild-type littermates were subjected to daily intraperitoneal injections of 50 mg kg^{-1} BrdU (BD Pharmingen) for 9 consecutive days (Extended Data Fig. 1a). Limbal and central corneal epithelial cells were harvested from *Abcb5* wild-type and *Abcb5* knockout mice either 24 h or 8 weeks after receiving the last BrdU injection. Limbal and central corneal epithelial cells were also harvested from age-matched untreated *Abcb5* wild-type and *Abcb5* knockout mice for use as experimental controls. Flow cytometry and immunohistochemistry staining were used to determine the frequency of BrdU-positive and BrdU-negative cells within epithelia of the limbus and central cornea. The threshold for BrdU positivity in the pulse chase experiments was determined using the background levels obtained from anti-BrdU antibody-stained limbal or

NIH-PA Author Manuscript

NIH-PA Author Manuscript

NIH-PA Author Manuscript

corneal epithelial cells from either wild-type or *Abcb5* knockout mice that did not receive any prior BrdU injections. These thresholds were used to establish the BrdU-positive gates shown in Extended Data Fig. 6a. An example of the controls used to set gates for BrdU positivity is shown in Extended Data Fig. 1b.

Human and murine corneal cell isolation

Cadaveric human corneoscleral tissues derived from consented donors according to Institutional Review Board (IRB)-approved protocols were obtained from Heartland Lions Eye Banks, Bascom Palmer Eye Institute, and Carver College of Medicine. After removal of the scleral rim, iris and trabecular meshwork, the limbus and central cornea were dissected under a microscope. Limbal and central corneal tissues were subsequently incubated with 2.4 units ml^{-1} Dispase II (Roche Diagnostics) at 37 °C for 1 h, followed by incubation with 0.5 M EDTA (Invitrogen) at 37 °C to recover the epithelial cells[21,22]. Murine limbal and corneal epithelial cells were obtained from *Abcb5* knockout and *Abcb5* wild-type mice. Immediately after euthanasia by CO_2 narcosis and subsequent eye enucleation, limbal and central corneal tissues were removed with microscissors under a dissecting microscope, placed in low Ca^{2+} keratinocyte serum free medium (KSFM, Invitrogen) and centrifuged for 5 min at 250*g* at 4 °C. After removal of the supernatant, tissue pellets were digested in 0.5% trypsin solution (Lonza)[23]. For transplantation experiments, $ABCB5^+$and $ABCB5^-$ limbal epithelial cells were isolated by FACS using ABCB5 monoclonal antibody labelling[11]. In brief, either human or murine limbal epithelial cells were labelled with primary ABCB5 monoclonal antibody (20 μg $μl^{-1}$) for 30 min at 4 °C, washed to remove excess antibody, followed by a 30 min incubation with secondary anti-mouse FITC-conjugated IgG. The $ABCB5^+$ and $ABCB5^-$ sorting gates were established on a Modified Digital Vantage cell sorter (Becton Dickinson and MGH Pathology Flow Cytometry Core, Simches Research Building) as shown in Extended Data Fig. 7. Only viable cells were selected for sorting by excluding all $DAPI^+$ cells (1 μg ml^{-1} DAPI, Sigma-Aldrich, added immediately before sorting) as identified using a 70 MW UV laser for excitation. The purity and viability of $ABCB5^+$ and $ABCB5^-$ sorted cells were established in representative post-sort analyses in which samples were re-analysed (Extended Data Fig. 7). $ABCB5^+$ cell purification resulted in a 255-fold increase for murine $ABCB5^+$ limbal cells (0.37% positivity before and 51% positivity after sorting; Extended Data Fig. 7h) and a 292-fold increase for human $ABCB5^+$ limbal cells (0.03% positivity before and 59% positivity after sorting; Extended Data Fig. 7h). $ABCB5^-$ cell enrichment resulted in complete absence of $ABCB5^+$ cells in both mouse and human samples (Extended Data Fig. 7h). Primary culture-expanded p63α-rich limbal epithelial cells for use in ABCB5 inhibition studies were purchased from Invitrogen (catalogue no. C-018-5C).

Flow cytometric analysis

Dual-colour flow cytometry was used to determine whether human $ABCB5^+$ limbal epithelial cells co-expressed p63α or KRT12 and whether murine $Abcb5^+$ limbal epithelial cells co-expressed Pax6 and Krt12, and was performed as described previously[11]. For human and murine ABCB5 and KRT12 co-expression analysis, cells were first incubated with mouse anti-ABCB5 monoclonal antibody, counterstained with goat anti-mouse FITC IgG, followed by incubation with goat polyclonal anti-KRT12 antibody and counterstaining

NIH-PA Author Manuscript NIH-PA Author Manuscript NIH-PA Author Manuscript

with Dylight 649 donkey anti-goat IgG. For human ABCB5 and p63α co-expression and murine Abcb5 and Pax6 co-expression analysis, cells were incubated with mouse anti-ABCB5 monoclonal antibody, counterstained with goat anti-mouse FITC IgG, permeabilized in BD Cytofix/Cytoperm Buffer (BD Biosciences), stained with either p63α or Pax6 antibodies, and counterstained with goat anti-rabbit Alexa 647 IgG. Washing steps with staining buffer or BD Perm/Wash Buffer (BD Biosciences) were performed between each step. Dual-colour flow cytometry was performed by acquisition of fluorescence emission at the Fl1 (FITC) and Fl4 (Alexa 647 and/or Dylight 649) spectra on a Becton Dickinson FACScan (Becton Dickinson), as described[11]. Murine Abcb5 and BrdU co-expression analysis was performed using the FITC BrdU Flow Kit (BD Biosciences), according to the manufacturer's instructions. Statistical differences between expression levels of the above-listed markers by $ABCB5^+$ and $ABCB5^-$cells were determined using the unpaired *t*-test. A two-sided *P* value of $P < 0.05$ was considered significant. For determination of the epithelial cell numbers in the central cornea and limbus of *Abcb5* wild-type and *Abcb5* knockout mice, dissociated single cell suspensions were stained with DAPI (1 μg ml^{-1} DAPI, Sigma-Aldrich) and analysed by flow cytometry using forward-scattered light (FSC) versus side-scattered light (SSC) to identify viable cells. Statistical differences between *Abcb5* wild-type and *Abcb5* knockout mice were determined using the unpaired *t*-test. A two-sided *P* value of $P < 0.05$ was considered significant.

Histopathology and immunohistochemical staining

To recover intact mouse ocular tissue, the whole decapitated mouse head was fixed in 4% PFA overnight, then eyes were enucleated with the lids attached, incubated in 30% sucrose in 1×PBS overnight at 4 °C, embedded in Tissue-Tek OCT compound (Sakura Finetek USA) and snap-frozen. Representative cryostat sections from each tissue block were stained with H&E. For immunofluoresence staining, cryostat sections (10 μm) were fixed in cold methanol for 10 min, blocked in 10% secondary serum plus 2% BSA in 1× PBS for 1 h, incubated with the primary antibody (or isotype control), followed by the appropriate secondary antibody for 1 h at room temperature. Following several washes, the slides were then coverslipped in hard-set mounting media with DAPI. Composite corneal photographs were assembled using Photoshop (Adobe) to overlay and match sequential images. Stitching was done by reducing the added photograph to 50% transparency, matching images, and returning the composite photograph to 0% transparency. The average number of epithelial cells per cornea (Fig. 2g) was determined by counting the number of DAPI-positive cells within the area defined by a 2 mm trephine in a composite photograph of a complete corneal section. At least three composite corneal sections were analysed per mouse, and five mice were analysed per group in four replicate experiments. The percentages of epithelial cells expressing Ki67 (Fig. 2j and Extended Data Fig. 6e), TUNEL (Fig. 2k) and Krt12 (Fig. 3a, b) were determined by counting the number of positive cells among the total number of DAPI-positive corneal epithelial cells using the techniques described earlier. Comparisons between the *Abcb5* wild-type and *Abcb5* knockout mice were performed using the unpaired *t*-test. The results of transplantation experiments were compared using the analysis of variance (ANOVA) test. Differences with $P < 0.05$ were considered statistically significant. For preparation of murine cornea whole mounts used for BrdU and Abcb5 immunostaining, whole mouse eyes with lids attached were enucleated, rinsed in PBS and immediately fixed

NIH-PA Author Manuscript

NIH-PA Author Manuscript

NIH-PA Author Manuscript

in 4% PFA overnight at room temperature. Fixed eyes were washed in PBS, the globe was bisected under a dissecting microscope in the nasal/temporal axis and the lids were removed. The posterior half of the eye was removed, leaving the cornea, limbus and part of the sclera intact. Relief cuts (7–10) were made from the corneal side and also from the scleral side to allow the limbus to lie as flat as possible. Throughout the dissection care was taken to handle the cornea and limbus as little as possible in order to retain anatomical integrity. To stain whole mount tissue for BrdU, tissue was placed on a rocker in 2 N HCl for 30 min, followed by 20 min in 0.1 M sodium borate. Two rinses in PBS were followed by 1 h in blocking buffer (25 ml 250 mg BSA, 2.5 ml 10× PBS, 1.5 ml goat serum, 75 μl Triton X-100, distilled H_2O). Two more PBS rinses were followed by overnight incubation with the following primary antibodies: rabbit anti-ABCB5 antibody (NBP1-77687, Novus) and biotinylated mouse anti-BrdU antibody (51-75512x, BD Pharmingen). Next, after two PBS rinses, tissue was incubated in blocking buffer for 15 min, washed twice in PBS, and incubated with secondary antibodies for 1 h (Alexa Fluor546 goat anti-rabbit and APC Streptavidin). Two more PBS rinses were followed by 5 min of DAPI incubation and two further PBS rinses. Tissue was then mounted on slides (Immu-Mount; Thermo-electron Incorporated) with spacers to preserve the morphology (Avery laser labels, 5,262 with holes punched for tissue) and subsequently coverslipped. Confocal microscopy was conducted on an inverted laser scanning confocal microscope system (FV1000, Olympus) with an automated stage (Prior Scientific) with ×20 (RI 0.85) and ×60 (RI 1.42) objectives.

Detection of palisades of Vogt and ABCB5 confocal microscopy

Optical coherence tomography (OCT) imaging of human corneal rims was performed with a prototype system as described previously by Lathrop *et al.*[24]. In brief, globes were punctured in several areas before the overnight fixation in 4% PFA. The following day, the tissue was washed and kept in PBS until ready to be embedded and sectioned. Prior to sectioning, the globes were scanned with a modified Bioptigen spectral-domain OCT system (Bioptigen; SuperLum) in order to define limbal regions containing defined palisade structures (Extended Data Fig. 1c–j). These palisade-containing regions were marked with a surgical pen (Extended Data Fig. 1c). Corneal and limbal tissues were then dissected from the marked areas (1 cm wide, extending 1 cm into the cornea and 1 cm into the sclera, see Extended Data Fig. 1i, j) and sunk in a sucrose solution (15%, then 30%) in order to preserve the tissue structure during embedding. Tissue sections were placed in moulds surrounded by cooled (4 °C) OCT compound (Tissue-Tek, Sakura Finetek USA) and frozen in liquid nitrogen. Thirty-micrometre palisade-containing sections were cut on a cryostat refrigerated microtome and placed on slides (Fisher Superfrost, Thermo Fisher Scientific). Prior to immunolabelling, slides were washed in distilled water 3× 15 min and once in $NaBH_4$ (1 mg ml^{-1}) for 10 min, and permeabilized with blocking buffer (1× PBS, 1% BSA, 0.3% Triton X-100, 6% donkey serum) for 1 h at room temperature. Slides were subsequently incubated in the dark at room temperature for 1 h with anti-ABCB5 monoclonal antibody (clone 3C2-1D12) diluted in dilution buffer (1× PBS, 1% BSA) and washed 3× 5 min each in blocking buffer. Alexa Fluor546 donkey anti-mouse antibody dissolved in dilution buffer was applied for 1 h at room temperature. Subsequently, three washes of blocking buffer were applied for 5 min each, followed by nuclear staining, washing 2× 5 min in 1× PBS and mounting with Immu-Mount (Thermo Electron

NIH-PA Author Manuscript

NIH-PA Author Manuscript

NIH-PA Author Manuscript

Corporation). Slides were examined by confocal microscopy conducted on an inverted laser scanning confocal microscope system (FV1000, Olympus) with an automated stage (Prior Scientific) using ×20 oil (RI 0.85) and ×60 (RI 1.42) objectives. The three-dimensional display of reconstructed stacks is available as Supplementary Video 3.

Antibodies

The following primary antibodies were used in flow cytometry experiments. Rabbit polyclonal anti-p63α antibody (H-129, sc-8344, Santa Cruz), rabbit polyclonal anti-p40 (DNp63) antibody (ABX-144A, Imgenex), mouse monoclonal anti-ABCB5 antibody (clone 3C2-2D12)[6], goat polyclonal anti-cytokeratin 12 antibody (L15, sc-17101, Santa Cruz), rabbit polyclonal anti-Pax6 antibody (PRB-278P, Covance), rabbit polyclonal IgG isotype control antibody (ab27478, Abcam), mouse IgG1κ isotype control antibody (clone X40, BD Biosciences), and goat IgG isotype control antibody (sc-3887, Santa Cruz). The secondary antibodies were goat anti-mouse FITC (F2012, Sigma-Aldrich), Alexa 647 goat anti-rabbit IgG (A21244, Invitrogen) and Dylight 649 donkey anti-goat (Jackson ImmunoResearch). For histopathology and immunohistochemical analyses, the following antibodies were used. Mouse monoclonal anti-ABCB5 (clone 3C2-1D12)[6] and rabbit antibody against p63α at 1:75 dilution (H-129, sc8344, Santa Cruz) followed by the appropriate secondary antibodies obtained from Jackson ImmunoResearch: FITC-donkey anti-rabbit (711-095-152) at 1:75 dilution or Alexa Fluor594 goat anti-mouse (115-515-062) at 1:250 dilution. In all cases, the isotype-matched antibodies rabbit IgG (550875, BD Pharmingen) and mouse IgG1κ isotype control antibody (clone X40, BD Biosciences) served as controls. Further antibodies used for histopathology and immunohistochemical analyses were as follows. Rabbit anti-ABCB5 antibody at 1:250 dilution (NBP1-50547, Novus), human anti-ABCB5 extracellular loop-associated peptide monoclonal antibody (clone 3B9, 5 μg ml^{-1}), rabbit polyclonal anti-Pax6 at 1:300 dilution (PRB-278P, Covance), goat anti-cytokeratin 12 (L15) at 1:50 dilution (sc17101, Santa Cruz), rabbit anti-human cytokeratin 12 (H-60, sc-25722), rabbit anti-cytokeratin 14 (AF64) at 1:1,000 dilution (PRB-155P, Covance), rabbit anti-Ki67 at 1:200 dilution (ab66155, Abcam), biotinylated BrdU antibody (51-75512, Pharmingen), followed by the appropriate secondary antibodies obtained from Jackson ImmunoResearch: donkey anti-goat Alexa Fluor488 at 1:250 dilution (705-545-003), donkey anti-rabbit Alexa Fluor594 at 1:20 dilution (711-585-152), goat anti-rabbit DyLight 549 at 1:250 dilution (111-504-144), or Cy3-donkey anti-rabbit at 1:250 dilution (711-165-152). Appropriate isotype-matched antibodies (rabbit IgG (550875, BD Pharmingen) and goat IgG (sc2028, Santa Cruz)) served as negative controls. Additional primary antibodies included rat anti-mouse Ly-6G 1:100 dilution (550291, BD Biosciences), rat anti-mouse F4/80 1:200 dilution (RM2900, Abcam), rat anti-mouse CD45R 1:25 dilution (550286, BD Biosciences), rabbit anti-CD3 1:100 dilution (5690, Abcam), rat IgG isotype control (559073, BD Pharmingen) and rabbit IgG isotype control (NB810-56910, Novus). Secondary antibodies were Alexa Fluor555 goat anti-rat at 1:250 dilution and Alexa Fluor594 goat anti-rabbit IgG at 1:250 dilution (A21434 and A11037 respectively, Life Technologies). Eyes from C57BL/6J mice taken 24 h post-infection with 500 colony forming units (c.f.u.) of *Staphylococcus aureus* and from normal C57BL/6J spleen and lymph nodes were used as positive controls for the reported inflammation marker expression studies. The fully human ABCB5 extracellular-loop-associated peptide-targeted IgG1 monoclonal antibody 3B9 was generated by Pfizer

NIH-PA Author Manuscript

NIH-PA Author Manuscript

NIH-PA Author Manuscript

Centers for Therapeutic Innovation (CTI) during a collaboration with Boston Children's Hospital using screening of a human scFv phage display library for selection of binders to biotin-peg2-ABCB5 peptide (RFGAYLIQAGRMTPEG; UniProt accession Q2M3G0), followed by sequence analysis and human IgG1 conversion. The monoclonal antibody 3B9 binds to human ABCB5 peptide (RFGAYLIQAGRMT PEG; UniProt accession Q2M3G0) and mouse Abcb5 peptide (RFGAYLIQAGRM MPEG; UniProt accession B5X0E4) at concentrations <10 nM, with no significant binding at these concentrations to either scrambled peptide or peptide homologues associated with the related ABCB1 (RFGAYLVAHKLMSFED; UniProt accession P08183), ABCB4 (RFGAYLIVNGHMRFRD; UniProt accession P21439) or ABC B11 (RYGGYLISNEGLHFSY; UniProt accession O95342) proteins. FITC-conjugated ZyMax goat anti-human IgG (H+L) antibody product (817111) was purchased from Invitrogen.

Cell viability assays

Human limbal epithelial cells were seeded on 96-well plates (15,000 per well, $n = 5$ replicates) and treated for 48 h with either blocking concentrations[12] of anti-ABCB5 monoclonal antibody clone 3C2-1D12 (ref. 6) or equivalent concentrations of isotype control monoclonal antibody (clone MOPC31C, Sigma). Cell viability was determined by the CellTiter-Glo Luminescent Cell Viability Assay (Promega) according to the manufacturer's instructions. In additional viability assays employing conditions resembling those used for $ABCB5^+$ cell staining for cell isolation, human limbal epithelial cells were incubated on ice with 2 μg ml^{-1} of anti-ABCB5 monoclonal antibody clone 3C2-1D12 (ref. 6) or isotype control monoclonal antibody (clone MOPC31C, Sigma) for 30 min. After washing with PBS, cells were seeded on 96-well plate (15,000 per well, $n = 5$ replicates) and grown at 37 °C for 48 h, followed by determination of cell viability as described earlier. Statistical differences between samples were determined using the unpaired *t*-test. A two-sided *P* value of $P < 0.05$ was considered significant.

Corneal fragility assay

Experimental animals were anaesthetized with intraperitoneal injections of 70 mg kg^{-1} sodium pentobarbital. Under a stereomicroscope, a partial epithelial defect was created in both eyes by brushing with a wet Microsponge (Alcon) as described by Kao *et al.*[25]. The animals were euthanized in a CO_2 chamber, and the corneas were removed and embedded in paraffin for histology. H&E-stained *Abcb5* knockout and wild-type corneas were analysed for the presence or absence of epithelial defects and results were compared using the Fisher's exact test. A two-sided *P* value of $P < 0.05$ was considered significant.

Corneal epithelial debridement

After anaesthesia with intraperitoneal injection of ketamine (120 mg kg^{-1} body weight; Hospira) and xylazine (10 mg kg^{-1} body weight; Burns Veterinary Supply), followed by topical application of one drop of 0.5% proparacaine eye drops (Akorn) into each eye, a 2 mm diameter epithelial wound was created by demarcating an area of the central cornea with a 2 mm trephine and removing the epithelium within the circle with a small scalpel, leaving the basement membrane intact. In each animal, the procedure was performed on the

NIH-PA Author Manuscript

NIH-PA Author Manuscript

NIH-PA Author Manuscript

right eye. Ak-Spore Ophthalmic Ointment (bacitracin zinc, neomycin sulphate and polymyxin B sulphate; Akorn) was applied to both eyes immediately after wounding and then twice per day for the next 48 h to prevent corneal infection and dryness. Analgesia was provided by subcutaneous injections of Buprenex (Reckitt Benckiser Pharmaceuticals) every 12 h for 48 h post-operatively at the dose of 1 mg kg^{-1}. Wound healing was monitored as described previously[26].

Corneal tight junction integrity

Hutcheon *et al.*[27] described a functional assay of corneal epithelial cell tight junction integrity using LC-biotin, which does not penetrate through the epithelium in the presence of intact tight junctions, whereas defective tight junctions allow penetration through the epithelium and into the corneal stroma. Wild-type and *Abcb5* knockout mice were assessed for corneal epithelial tight junctions using the LC-biotin staining method performed as described[28]. In brief, LC-biotin staining solution was prepared by dissolving 1 mg ml^{-1} EZ-Link-Sulfo-NHS-LC-Biotin (Pierce) in Hank's balanced salt solution (HBSS, Lonza) plus 2 mM $MgCl_2$ and 1 mM $CaCl_2$. This solution was applied to the cornea of wild-type and knockout mice for 15 min at the time of euthanasia. Eyes were rinsed with PBS (Lonza), enucleated and placed in Tissue-Tek OCT (Sakura Finetek) for frozen sectioning. Sections of wild-type and knockout corneas were stained with FITC-streptavidin to detect the presence of LC-biotin.

Transplantation experiments

Murine donor limbal epithelial cells were transplanted onto the eyes of syngeneic C57BL/6J recipient mice with an induced limbal stem cell deficiency. Human donor limbal epithelial cells were transplanted onto the eyes of immunodeficient NOD.Cg-*Prkdc*^{scid} *Il2rg*^{tm1Wjl}/SzJ (NSG) mice with an induced limbal stem cell deficiency. Four types of donor transplants were performed: (1) $ABCB5^+$ limbal epithelial cells; (2) $ABCB5^-$ limbal epithelial cells; (3) unsegregated limbal epithelial cells; and (4) grafts containing no cells (fibrin gel carrier only). Twenty-four hours before transplantation, murine and human donor cells were seeded onto a fibrin carrier, which was prepared by dissolving fibrinogen and thrombin stock solutions (TISSUCOL-Kit Immuno, Baxter) in 1.1% NaCl and 1 mM $CaCl_2$ to a final concentration of 10 mg ml^{-1} fibrinogen and 3 IU ml^{-1} thrombin as described[29]. On the day of transplantation, total LSCD was induced in anaesthetized recipient mice by removing the corneal and limbal epithelium with an Algerbrush II corneal rust ring remover with a 0.5 mm burr (AMBLER Surgical)[30]. Following induction of LSCD, recipient mice received fibrin gel carrier-based transplants that were secured via four subconjunctival sutures. Eyelids were sutured with 8-0 nylon sutures to keep the eyes closed. Ak-Spore Ophthalmic Ointment (bacitracin zinc, neomycin sulphate and polymyxin B sulphate; Akorn) was applied on both eyes immediately after wounding and then twice per day for the next 48 h to prevent corneal infection and dryness. Analgesia was provided by subcutaneous injections of 5–10 mg kg^{-1} Metacam (Boehringer Ingelheim Pharmaceuticals), given preoperatively and by subcutaneous injections of 0.05–0.1 mg kg^{-1} of Buprenex (Reckitt Benckiser Pharmaceuticals) every 12 h for 24 h post-operatively. In addition, after surgical recovery mice were also treated with anti-inflammatory Inflanefran Forte eye drops (Allergan) for the first 5 days, and then with 1% Avastin (Bevacizumab, Genentech) eye drops daily for 5

NIH-PA Author Manuscript

NIH-PA Author Manuscript

NIH-PA Author Manuscript

days. Slit lamp examination was performed weekly until euthanasia. Eyes were enucleated postmortem and fixed in 10% buffered formalin for methacrylate embedding (Technovit, Heraeus Kulzer) or snap-frozen in Tissue-Tek OCT (Sakura Finetek).

Confocal and multiphoton microscopic analysis of corneas

For whole corneal imaging, animals were euthanized and their eyes carefully enucleated. The eyes were then mounted using cyanoacrylate glue with the cornea facing up. Whole corneal imaging was performed using a custom-built video-rate laser-scanning confocal and multiphoton microscope with a custom femtosecond laser supply based on systems described by Veilleux et al.31 and Wang et al.32). In brief, a 1,550 nm turnkey fibre-based laser (Calmar Laser) with a 5 MHz pulse repetition rate and 360 fs pulse width was frequency doubled using a bismuth borate (BiBO) crystal with an AR1550/775nm coating (Newlight Photonics) to generate ~7.5 mW at the focal plane. Corneal layers were imaged using confocal reflectance with a quarter wave plate and an avalanche photodiode module (Hamamatsu) to collect backscattered signal. To further probe the structural elements of the cornea, second harmonic generation of collagen fibrils was collected using a PMT and a 390/40 nm band pass filter (Semrock). The apex of each cornea was imaged using a ×60 1.0 NA objective (Olympus) at 15 frames per second with 1 μm steps from the surface of the cornea through the basal epithelial layers.

Statistical analysis

We established a provisional number of mice per cohort for the pilot phase of a particular experiment based on initial feasibility considerations with regard to availability of cell graft material, and, if the data were suggestive of a significant difference, we calculated the numbers of mice needed for a repeat experiment to establish statistical significance, or not. There was no exclusion of samples or animals from the analysis. The investigators were blinded when assessing experimental outcomes. In gene knockout analyses, animals were allocated to experimental groups based on their *Abcb5* knockout or *Abcb5* wild-type status. For transplantation experiments all recipient animals were randomly assigned to their respective experimental groups. Two-sided tests were used in the statistical analyses. Appropriate statistical tests were used for all data sets depicted in the figures, with data meeting the assumptions of the tests. Variations within each group of data were estimated and similar between statistically compared groups. $*P < 0.05$, $** P < 0.01$ and $***P < 0.001$.

NIH-PA Author Manuscript
NIH-PA Author Manuscript
NIH-PA Author Manuscript

Extended Data

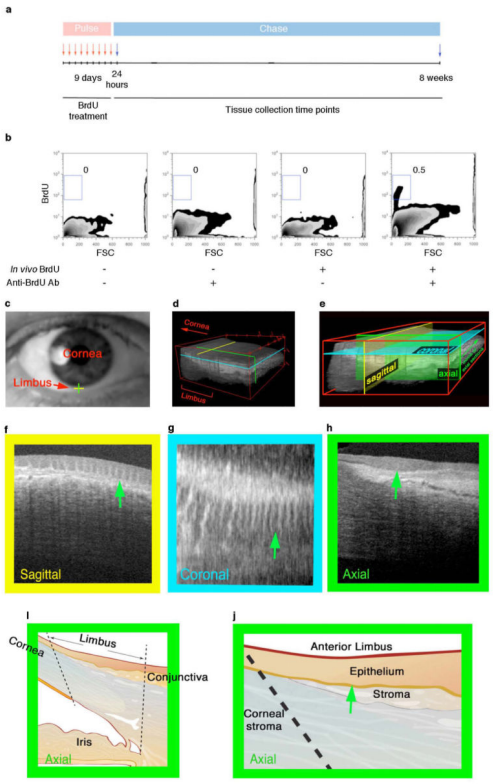

Extended Data Figure 1. BrdU label-retaining cells and optical coherence tomography identification of the palisades of Vogt

a, Schematic summary of the experimental design for BrdU pulse-chase experiments. **b**, Representative flow cytometric analyses depicting specific staining of BrdU label-retaining cells in limbal epithelial cells of wild-type mice that did not receive BrdU (left two panels) or wild-type mice that received BrdU followed by an 8-week chase (right two panels). Limbal epithelial cells were recovered and stained with either anti-BrdU antibody or with an isotype control antibody. The percentages of BrdU-positive cells within the gate are indicated on each plot. **c**–**e**, Schematic illustration of the optical coherence tomography (OCT) imaging algorithm used for the human limbus. **f**–**h**, Cross-sectional images of human cornea depicting a sagittal view (**f**), a coronal C-mode image reconstructed to reveal the palisades (green arrow) and the rete pegs (**g**), and an axial view of the corneolimbal junction showing the conjunctival stroma beneath the limbal epithelium (green arrow identifies the basal epithelial layer) (**h**). **i**, **j**, Schematic representation of the limbus (**i**) and the anterior limbus (**j**), illustrating the orientation of OCT images used to identify and dissect palisade-rich regions within the limbus of corneal rims (approximately 1 cm^2 tissue blocks). These smaller sections were then stained with anti-ABCB5 monoclonal antibody and analysed by confocal microscopy, as is shown in Fig. 1e of the main manuscript. Supplementary Video 3 consists of sequential confocal images depicting the location of $ABCB5^+$ cells within palisades.

NIH-PA Author Manuscript
NIH-PA Author Manuscript
NIH-PA Author Manuscript

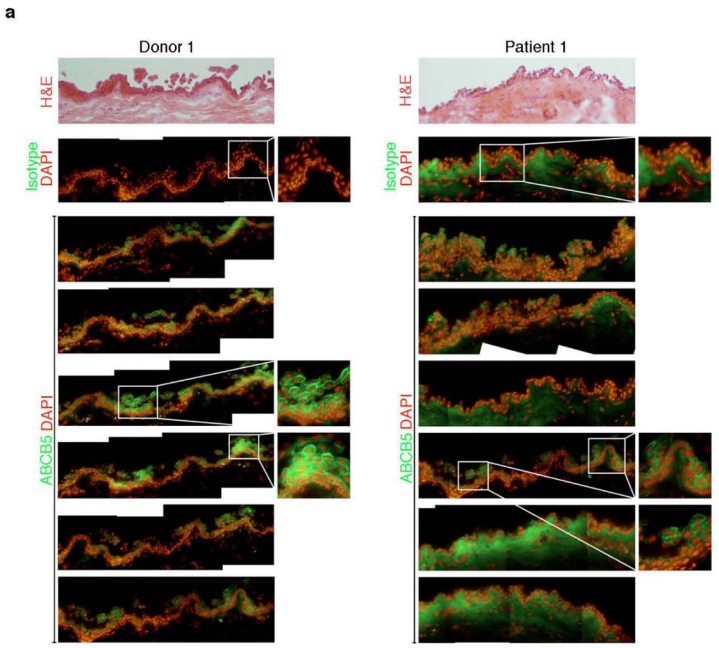

c

Patient	Gender	Age	Cause of LSCD	Other Pathology	Previous surgery	Procedure
1*	Male	46	Chemical burn - OD	Glaucoma suspect OD	None	KLAL+PKP
2**	Female	31	Autoimmune corneal melt; PUK with partial LSCD	Multiple graft failure OD Retinal vasculitis OD	2xPKPs Cataract surgery	KLAU

Extended Data Figure 2. Limbal biopsies from normal donors or patients with LSCD

a–**c**, Limbal biopsies were obtained from normal donors or patients with LSCD. **a**, Typical findings are shown for a patient (patient 1) with a chemical burn before receiving a penetrating keratoplasty plus kerato-limbal allograft from a cadaveric donor eye (donor 1). Serial cross-sections of the biopsies were stained with either H&E, isotype control monoclonal antibody, or ABCB5 moncolonal antibody. ABCB5 staining in the limbal epithelium of donor 1 reveals nests of ABCB5-positive cells, whereas ABCB5-positivity is reduced in the limbal epithelium of patient 1. Photographs of immunofluorescent staining

NIH-PA Author Manuscript

NIH-PA Author Manuscript

NIH-PA Author Manuscript

are montages of sequential photos at ×20 magnification. In these studies, equal-sized biopsies were recovered from a portion of the patient and donor limbus, frozen, and sectioned to produce eight sequential sections. All epithelial cells were counted in each section. A total of 2,031 and 2,051 epithelial cells were counted in patient 1 and donor 1, respectively. **b**, Limbal biopsies were obtained from a patient (patient 2) with an autoimmune corneal melt, peripheral ulcerative keratitis, and partial limbal stem cell deficiency before receiving a kerato-limbal autograft from the patient's normal contralateral eye (donor 2). Serial sections of the biopsies were stained with either H&E, isotype control monoclonal antibody, or ABCB5 monoclonal antibody. ABCB5 positivity was present in the basal layer of the limbal epithelium of donor 2, while a dramatically reduced epithelial layer and no ABCB5 staining was observed in the limbus of patient 2. Photographs of immunofluorescent staining are montages of sequential photos at ×20 magnification. In these studies, equal-sized biopsies were recovered from a portion of the patient and donor limbus, frozen, and sectioned to produce eight sequential sections. All epithelial cells were counted in each section. A total of 563 and 2,662 epithelial cells were counted in patient 2 and donor 2, respectively. Patient 2 had a reduced number of epithelial cells due to the extensive damage from chronic autoimmunity. **c**, LSCD patient information. *Donor 1: cadaveric donor; **Donor 2: autologous transplant from contralateral eye. KLAL, kerato-limbal allograft (limbal tissue was harvested from donor eye); KLAU, kerato-limbal autograft (part of limbal tissue was resected from uninjured contralateral eye); OD, right eye; PKP, penetrating keratoplasty; PUK, peripheral ulcerative keratitis.

NIH-PA Author Manuscript
NIH-PA Author Manuscript
NIH-PA Author Manuscript

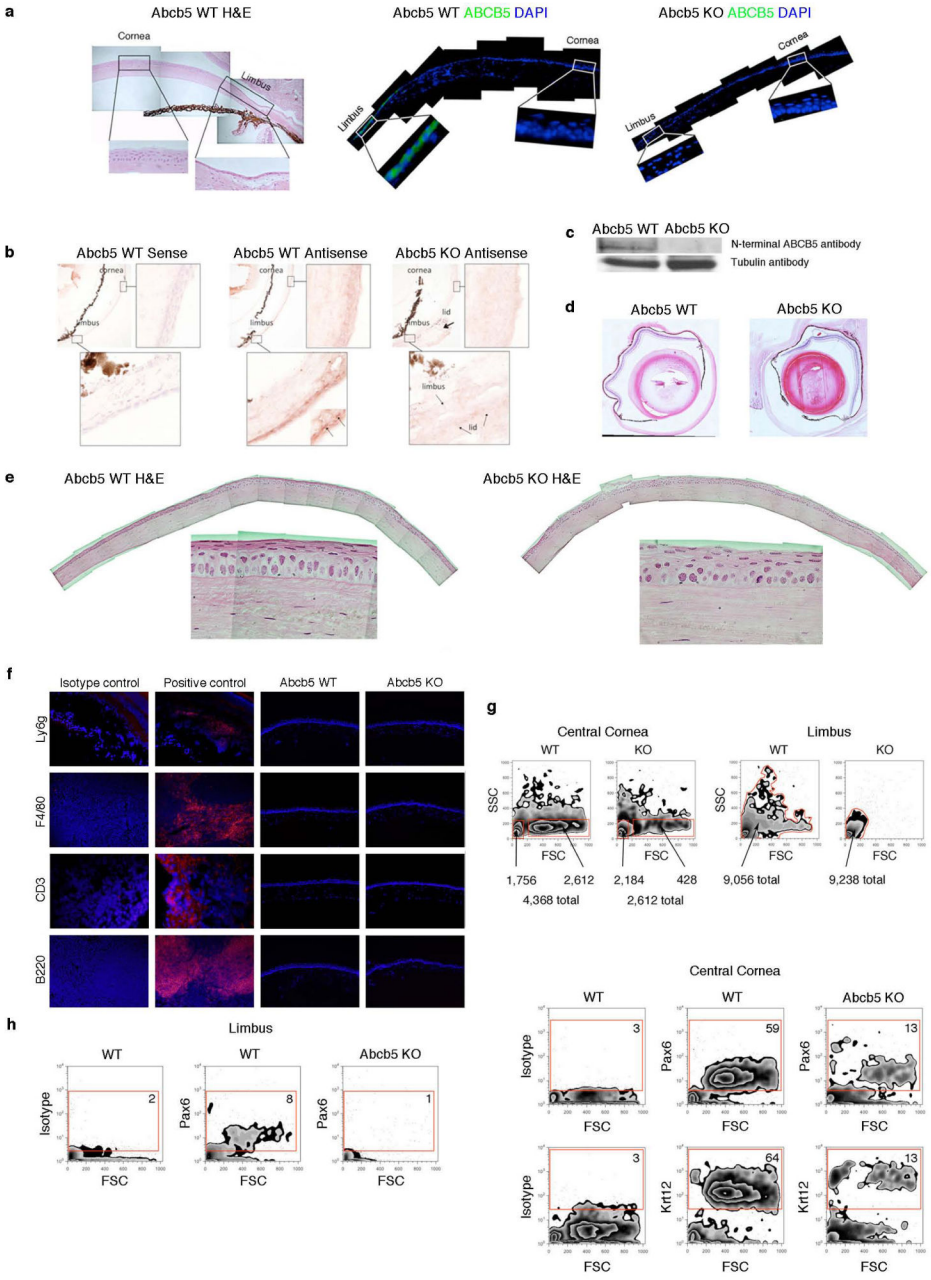

Extended Data Figure 3. Phenotypic evaluation of Abcb5 knockout versus wild-type mice

a, H&E staining of the normal murine eye depicts location of the limbus and central cornea (left panel). Representative immunofluorescence staining of the wild-type (WT) murine eye illustrates the presence of an Abcb5^{+} cell population (green) in the limbus but not the central cornea (middle panel). *Abcb5* immunofluorescence staining of the knockout (KO) mouse demonstrates loss of *Abcb5* expression in the limbus (right panel). **b**, *In situ* hybridization with murine antisense or sense Abcb5 mRNA probes spanning 144 bp of murine *Abcb5* cDNA encoding exon 10 of the murine Abcb5 gene (GenBank accession number JQ655148) reveals loss of Abcb5 mRNA expression in *Abcb5* knockout mice. **c**, Western blot analyses

NIH-PA Author Manuscript

NIH-PA Author Manuscript

NIH-PA Author Manuscript

of murine protein lysates with rabbit polyclonal antibody directed against the *Abcb5* N terminus (Abgent) reveal loss of a ~80 kDa protein band of the predicted size in *Abcb5* knockout mice. **d**, H&E cross-section of a wild-type eye (left) and an *Abcb5* knockout eye (right) depicts a normal shape of the *Abcb5* knockout eye and the presence of all major structures including cornea, conjunctiva, iris, lens and retina. **e**, H&E staining of methacrylate-embedded *Abcb5* wild-type (left) and *Abcb5* knockout (right) age-matched adult corneas. **f**, Inflammatory cell marker immunostaining and respective isotype control immunostaining in positive control tissues (left columns) and inflammatory cell marker immunostaining of *ABCB5* wild-type and *ABCB5* knockout corneas (right columns). Ly-6G, neutrophil marker; F4/80, macrophage marker; CD3, T-cell marker; B220, B-cell marker. Positive control tissues: *Staphylococcus aureus*-infected murine cornea (Ly-6G); murine spleen (F4/80 and B220); murine lymph node (CD3). **g**, Representative flow cytometry analyses of either the central corneal (left) or the limbal (right) epithelium of wild-type and *Abcb5* knockout mice. Forward scatter (FSC) and side scatter (SSC) indicate cellular size and granularity, respectively. The central corneal epithelium of *Abcb5* knockout mice showed reduced numbers of epithelial cells compared to wild-type epithelium (left panels), caused by a reduction in larger cells (right gates), but not smaller cells (left gates). There was no reduction in the numbers of limbal epithelial cells (right panels). Representative results of samples pooled from four eyes are shown ($n = 3$ experiments). **h**, Representative flow cytometry analyses of epithelial cells harvested from either the limbus or the central cornea of wild-type and *Abcb5* knockout mice. Recovered cells were stained with isotype control antibody, anti-Pax6 antibody, or anti-Krt12 antibody. There was a reduced frequency of $Pax6^+$ cells in the limbus of *Abcb5* knockout mice and a reduced frequency of $Pax6^+$ and $Krt12^+$ epithelial cells in the central cornea of *Abcb5* knockout mice. Red gates identify $Pax6^+$ or $Krt12^+$ cells compared to isotype control staining. Representative plots of $n = 3$ experiments for each marker are shown. Magnification in **a**, **b**, **e**, **f**: ×20; **d**: ×4.

NIH-PA Author Manuscript

NIH-PA Author Manuscript

NIH-PA Author Manuscript

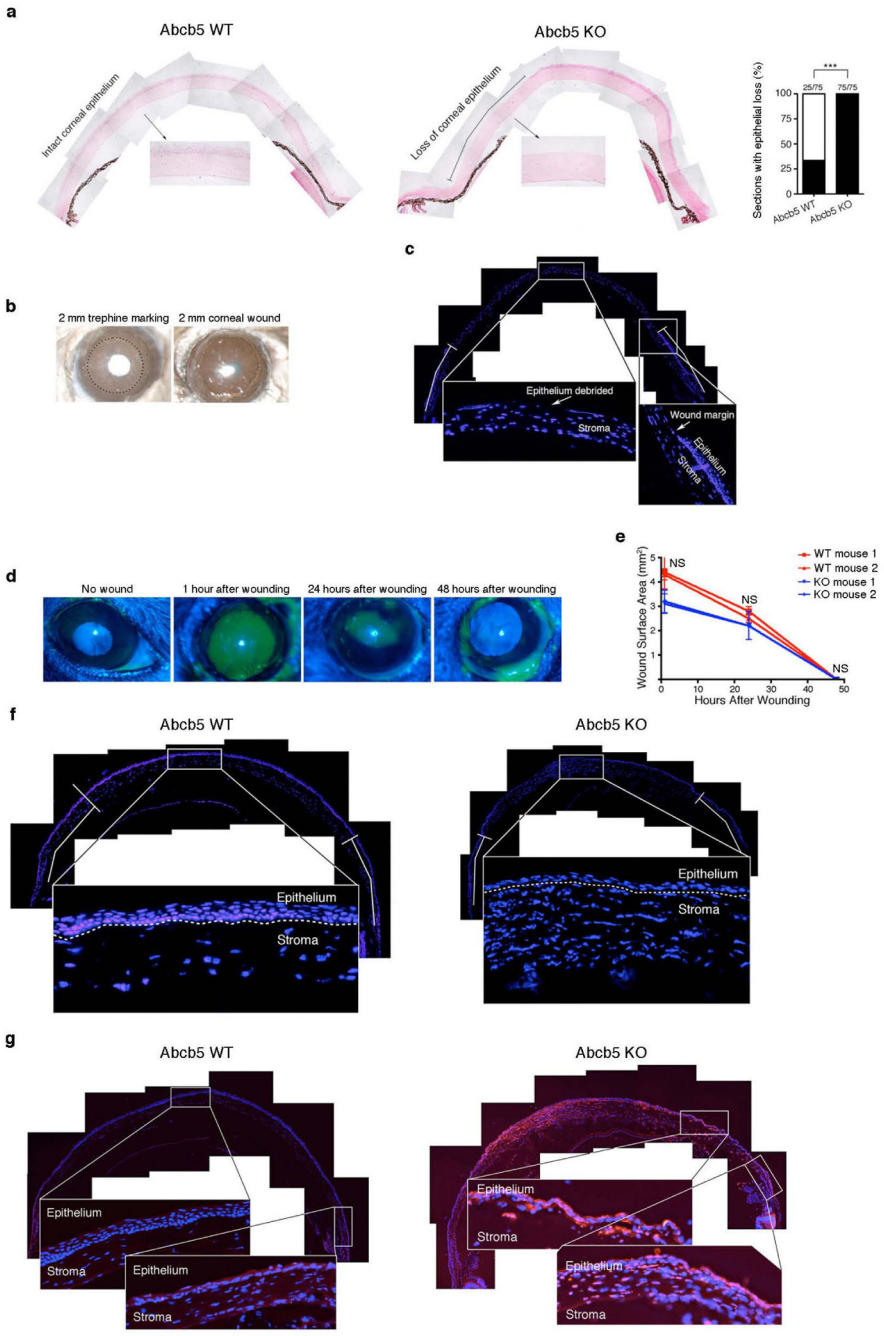

Extended Data Figure 4. Functional evaluation of *Abcb5* knockout versus wild-type mice

a, Increased corneal fragility in *Abcb5* knockout mice. H&E-stained sections of wild-type (WT) and *Abcb5* knockout (KO) corneas collected immediately after brushing with a wet Microsponge were examined for the presence or absence of epithelial defects. Only 33% of wild-type animal-derived cornea sections exhibited small epithelial defects (< 25% of epithelium), whereas 100% of *Abcb5* knockout cornea sections exhibited significant epithelial injury (n = 3 mice per group, 25 sections per mouse, Fisher's exact test: P < 0.001). **b**–**e**, Wound healing following corneal epithelial debridement of wild-type and

NIH-PA Author Manuscript

NIH-PA Author Manuscript

NIH-PA Author Manuscript

Abcb5 knockout mice. **b**, The area to be debrided was marked with a 2 mm trephine and the epithelium was removed with a small scalpel. **c**, DAPI-stained cross-section of the cornea immediately following central epithelial debridement depicting the wound margins and exposed central corneal stroma. Image is a montage of sequential photos at ×10 magnification. **d**, Corneal epithelial wound closure was monitored at 1, 24, and 48 h post-debridement via fluorescein staining. **e**, Wound closure rates were not significantly different between wild-type and *Abcb5* knockout mice (summary of $n = 2$ replicate experiments, $n = 4$ mice per group, unpaired t-test, P = not significant). **f**, Reduced re-epithelialization of wounded corneas in *Abcb5* knockout mice. Representative DAPI-stained composite corneal cross sections of wild-type (left) and *Abcb5* knockout (right) mice 48 h after a corneal epithelial debridement wound, demonstrating a reduced number of epithelial cells in *Abcb5* knockout mice. The white dashed line demarcates the epithelium from stroma; the white box indicates area shown at ×20 magnification (montage pictures are at ×10 magnification); white lines demarcate the area in which epithelial cells were counted. Epithelial cells were counted within the standardized area in at least three consecutive composite cross sections in three replicate mice per group in two separate experiments (aggregate data shown in Fig. 2i). **g**, Increased apoptosis in wounded corneas of *Abcb5* knockout mice. Representative TUNEL-stained composite corneal cross-sections of wild-type (left) and *Abcb5* knockout (right) mice 48 h after a corneal epithelial debridement wound, demonstrating increased numbers of apoptotic cells in *Abcb5* knockout mice. Areas defined by the white box are shown at ×20 magnification (montage pictures at ×10 magnification). The number of TUNEL-positive epithelial cells was counted, and the data from two replicate experiments in $n = 2$ mice are summarized in Fig. 2k. Error bars indicate s.e.m. NS, not significant.

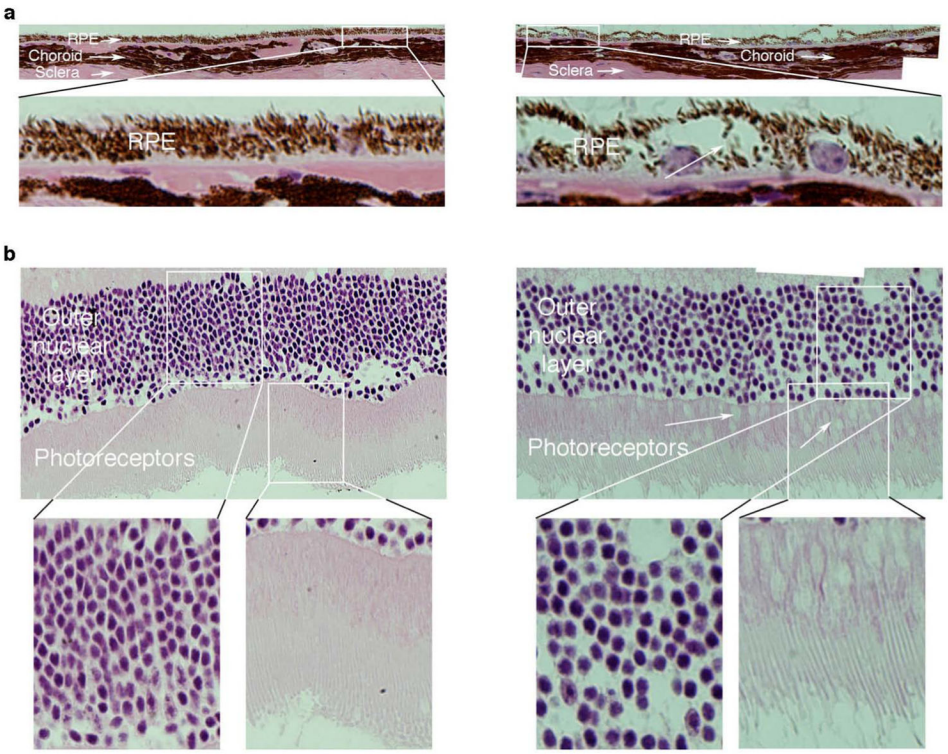

NIH-PA Author Manuscript
NIH-PA Author Manuscript
NIH-PA Author Manuscript

Extended Data Figure 5. Phenotypic characterization of wild-type versus *Abcb5* knockout retina

Analysis of H&E-stained sections from 9-month-old wild-type mice (left) or *Abcb5* knockout mice (right) revealed changes in the retina and retinal pigment epithelial cells (RPEs). **a**, Compared to wild-type mice (left), RPEs in *Abcb5* knockout mice (right) were enlarged and distended, possibly due to the presence of vacuoles. **b**, Compared to wild-type mice (left), areas of abnormal RPE in *Abcb5* knockout eyes (right) coincided with changes in the overlaying photoreceptors and the outer nuclear layer. There was a thinning and attenuation of photoreceptor outer segments along with a disruption of inner segments, which was associated with a loss of cells in the outer nuclear layer. Magnification: ×20.

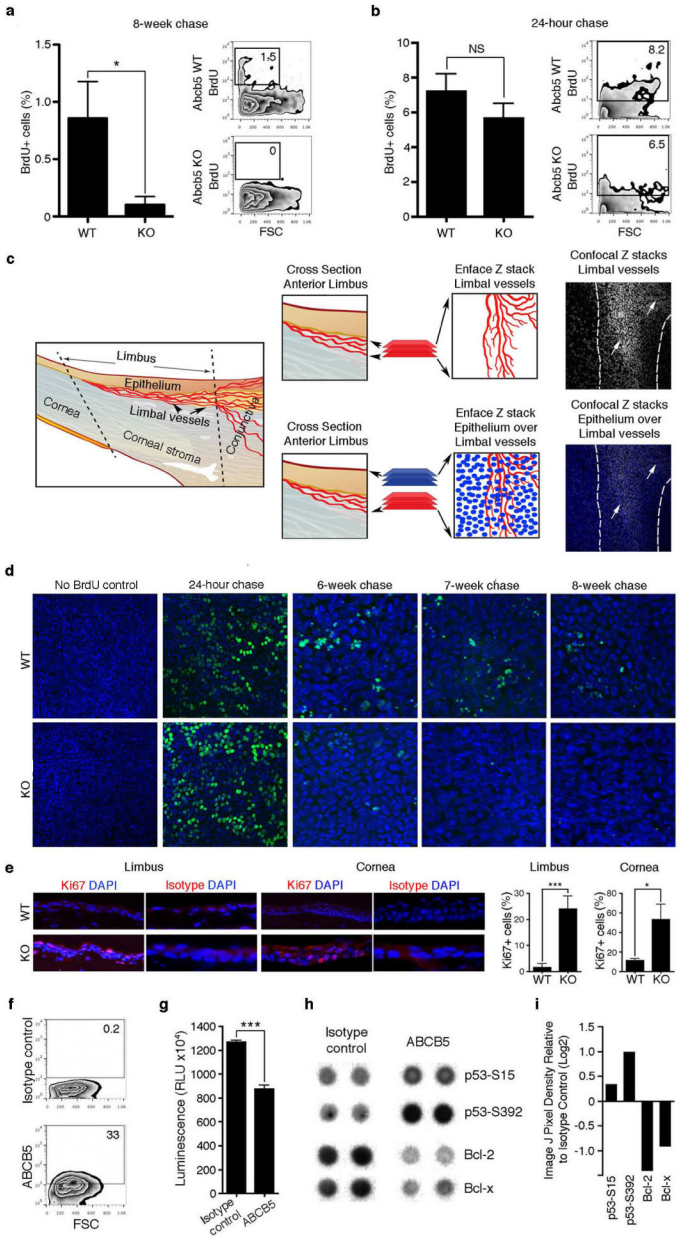

NIH-PA Author Manuscript

NIH-PA Author Manuscript

NIH-PA Author Manuscript

Extended Data Figure 6. ABCB5 regulates LSC quiescence and functions as an anti-apoptotic molecule

a, Flow cytometric analysis showing depletion of BrdU label-retaining cells in *Abcb5* knockout (KO) versus *Abcb5* wild-type (WT) limbal epithelial cells after an 8-week chase. Analysis was performed in $n = 6$ *Abcb5* wild-type mice and in $n = 12$ *Abcb5* knockout mice. The experiment was performed three times. Data were analysed using the unpaired *t*-test. Data are shown as mean ± s.e.m., $P < 0.05$. **b**, Equivalent BrdU labelling in *Abcb5* wild-type and *Abcb5* knockout mice after a 24 h chase is shown (mean ± s.e.m.). The experiment was performed using $n = 4$ mice per group and was performed twice. Data were analysed using the unpaired *t*-test, *P* = not significant. **c**, Schematic illustrating identification of the limbal epithelium within corneal whole mounts via identification of posteriorly localized limbal vessels within the underlying stroma. Far right, confocal Z-stack images displaying limbal vessels alone (top, white arrows) and limbal vessels (white arrows) with overlying limbal epithelium (bottom) (see also Supplementary Video 2). **d**, Sequential immunofluorescence histological examination of limbal epithelium in corneal whole mounts (localized as illustrated in **c** and Supplementary Video 2), showing equivalent BrdU incorporation after a 24 h chase in *Abcb5* knockout and wild-type mice (column 2), but progression to selective loss of BrdU label-retaining cells in *Abcb5* knockout mice at the 8-week chase time point (far right column). Far left column, negative BrdU immunostaining result (negative control) of BrdU-untreated wild-type and *Abcb5* knockout mouse limbal epithelium. **e**, Immune fluorescence analysis of Ki67 expression in *Abcb5* wild-type and *Abcb5* knockout mouse limbus and cornea. Bar graphs on the right illustrate the percentage of $Ki67^+$ cells in *Abcb5* wild-type versus *Abcb5* knockout mice in the limbus and cornea. The percentages of $Ki67^+$ cells in *Abcb5* wild-type versus *Abcb5* knockout mice in the limbus and cornea were determined using $n = 4$ mice per group. The experiment was performed twice. Within a standardized area, all corneal epithelial cells were counted in at least three consecutive cross-sections. Data were analysed using the unpaired *t*-test. Data are shown as mean ± s.e.m. **f**, Flow cytometric analysis of ABCB5 expression by p63α-rich human limbal epithelial cells. **g**, Cell viability measured in relative luciferase units (RLU) following 48 h of ABCB5 monoclonal antibody or isotype control monoclonal antibody treatment ($n = 5$ experimental replicas, mean ± s.e.m.). Data were analysed using the unpaired *t*-test, $P < 0.001$. **h**, **i**, Differential expression of apoptosis pathway-associated proteins detected by Proteome Profiler Apoptosis Array (ARY009, R&D Systems) following ABCB5 monoclonal antibody or isotype control monoclonal antibody treatment, analysed using ImageJ software. Error bars indicate s.e.m. $*P < 0.05$, $***P < 0.001$. NS, not significant. Magnification in **c**–**e**: ×20.

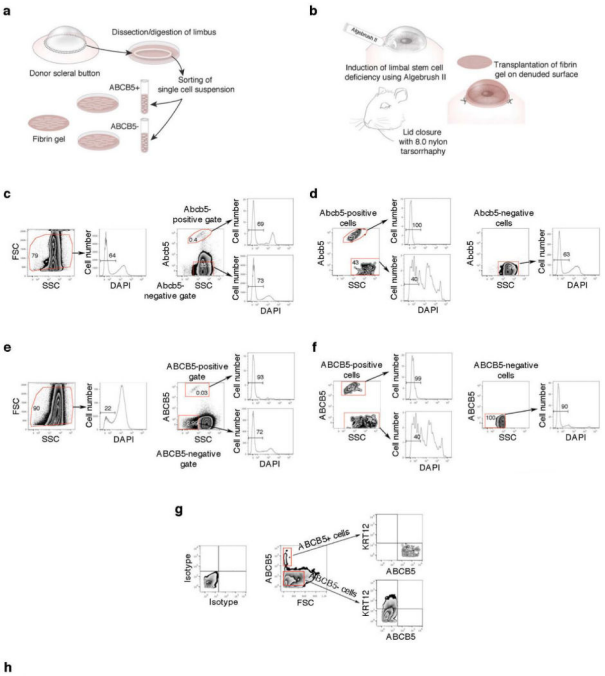

h

Donor	Unsegregated grafts 500 cells/graft/mouse		ABCB5(+) enriched grafts 500 cells/graft/mouse		ABCB5(-) enriched grafts 500 cells/graft/mouse	
Mouse limbus	ABCB5		ABCB5		ABCB5	
	Positive	Negative	Positive	Negative	Positive	Negative
Viable cells/graft	1	319	255	86	0	312
Human limbus	ABCB5		ABCB5		ABCB5	
	Positive	Negative	Positive	Negative	Positive	Negative
Viable cells/graft	1	109	292	80	0	450

Extended Data Figure 7. Limbal stem cell transplantation protocol and cell sorting for purification of ABCB5$^+$ and ABCB5$^-$ limbal epithelial cells

a, Recovery and separation of ABCB5$^+$ and ABCB5$^-$ limbal epithelial cells from donor corneas followed by preparation of fibrin gels containing donor cells. **b**, Induction of limbal stem cell deficiency in recipient mice and transplantation of donor grafts. **c**, **e**, Representative flow cytometry analyses showing sorting gates and viability of murine (**c**) and human donor limbal epithelial cells (**e**). **d**, **f**, Post-sort analysis depicting the purity and viability of ABCB5$^+$-enriched and ABCB5$^-$-enriched subpopulations of limbal epithelial cells isolated from mice (**d**) and human donors (**f**). Viability is shown as the percentage of cells excluding DAPI. **g**, KRT12 expression in ABCB5$^+$ and ABCB5$^-$ limbal cell populations. **h**, Number and viability of donor cells used for transplantation.

NIH-PA Author Manuscript NIH-PA Author Manuscript NIH-PA Author Manuscript

NIH-PA Author Manuscript

NIH-PA Author Manuscript

NIH-PA Author Manuscript

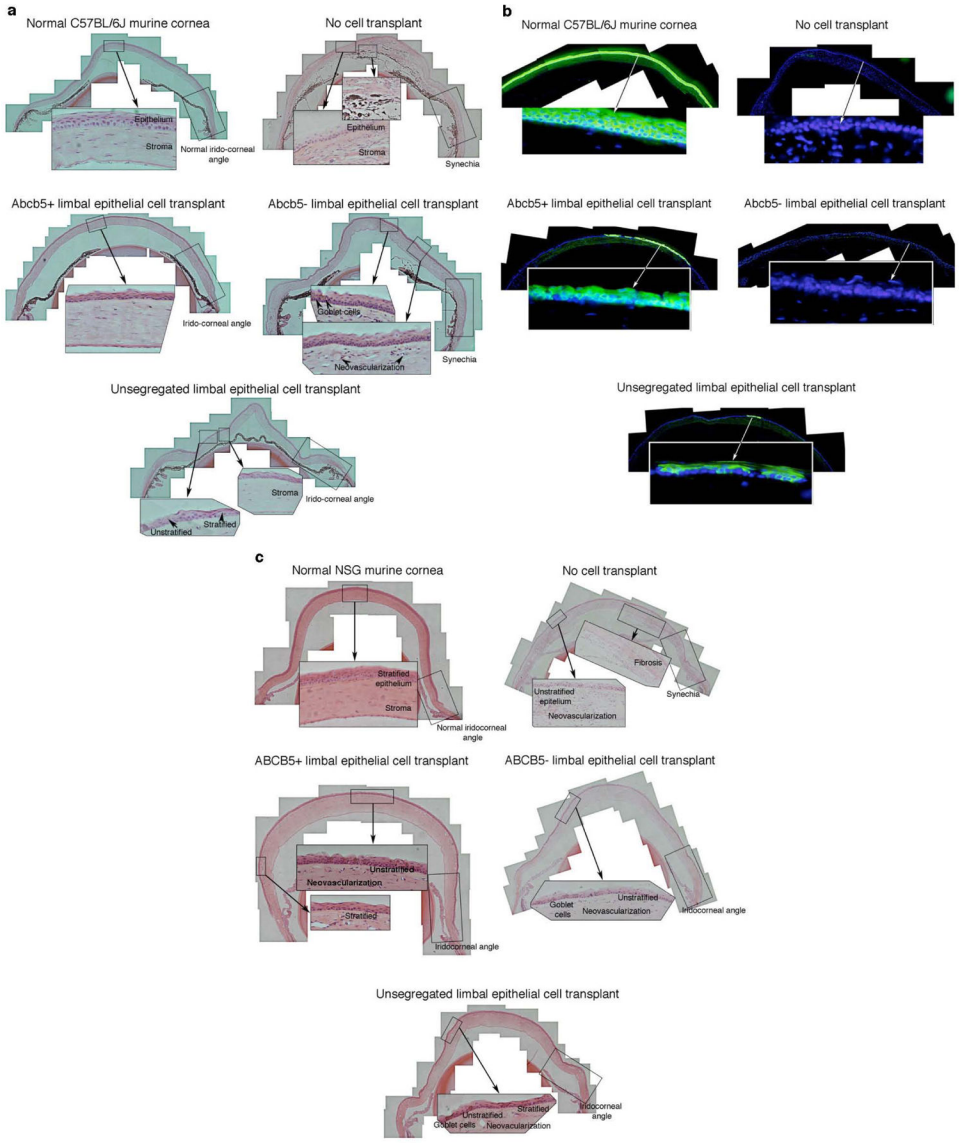

Extended Data Figure 8. Restoration of LSCD by donor murine Abcb5^{+} or human ABCB5^{+} cell transplants

Representative H&E composite corneal cross-sections of recipient C57BL/6J mice 5 weeks after receiving an induced LSC deficiency followed by engraftment of donor fibrin gel transplants containing the following syngeneic murine limbal epithelial cell subpopulations: (1) no cells (negative control), (2) Abcb5^{+} cells, (3) Abcb5^{-} cells, or (4) unsegregated cells. A normal untreated cornea (no LSCD) served as a positive control. The positive control displays the typical stratified corneal epithelium and iridocorneal angle. Mice receiving transplants with no cells displayed the typical conjunctivalization that occurs following a LSCD, that is, unstratified conjunctival epithelium covers the cornea with extensive inflammation, neovascularization, and stromal oedema. Synechia (where the iris adheres to the cornea) is typical of intense anterior segment inflammation. In contrast, mice that received transplants of Abcb5^{+} cells, but not Abcb5^{-} cells, displayed a restored stratified

NIH-PA Author Manuscript

NIH-PA Author Manuscript

NIH-PA Author Manuscript

corneal epithelium with no evidence of inflammation, neovascularization, stromal oedema, or synechia. Mice that received transplants of unsegregated limbal epithelial cells displayed areas of stromal oedema with unstratified epithelium, while other parts of the cornea contained normal stratified epithelial cells. **b**, Restoration of Krt12 expression by donor murine Abcb5^{+} cell transplants. Representative immunofluorescent Krt12 staining (green) of recipient C57BL/6J mice 5 weeks after an LSCD induction followed by transplantation of donor fibrin gel grafts containing grafts as in **a**. Normal untreated murine cornea (no LSCD), shown here as a positive control, displays high intensity of Krt12 staining. Mice that received grafts containing no cells displayed no Krt12 expression. In contrast, mice transplanted with Abcb5^{+} cells, exhibited significantly enhanced Krt12 expression in comparison to the mice transplanted with unsegregated limbal epithelial cells. No Krt12 expression was detected in the mice transplanted with Abcb5^{-} cells. The white box depicts the area shown at ×40 magnification. Montage images are shown at ×10 magnification. **c**, Restoration of LSCD by donor human ABCB5^{+} limbal cell transplants. Representative H&E composite corneal cross-sections of recipient immunodeficient NSG mice 5 weeks after LSCD induction followed by transplantation of donor fibrin gel grafts containing the following human limbal epithelial cell subpopulations: (1) no cells (negative control), (2) ABCB5^{+} cells, (3) ABCB5^{-} cells, and (4) unsegregated cells. The positive control (normal untreated NSG cornea (no LSCD)) displays the typical stratified corneal epithelium and iridocorneal angle. Mice that received transplants with no cells displayed evidence of conjunctivalization that occurs following a LSC deficiency; that is, unstratified conjunctival epithelium covers the cornea with extensive neovascularization and synechia (anterior segment inflammation is muted in NSG mice due to their immunodeficiency). In contrast, mice that received transplants containing ABCB5^{+} cells displayed areas of restored stratified epithelium, whereas recipients receiving ABCB5^{-} cell grafts did not.

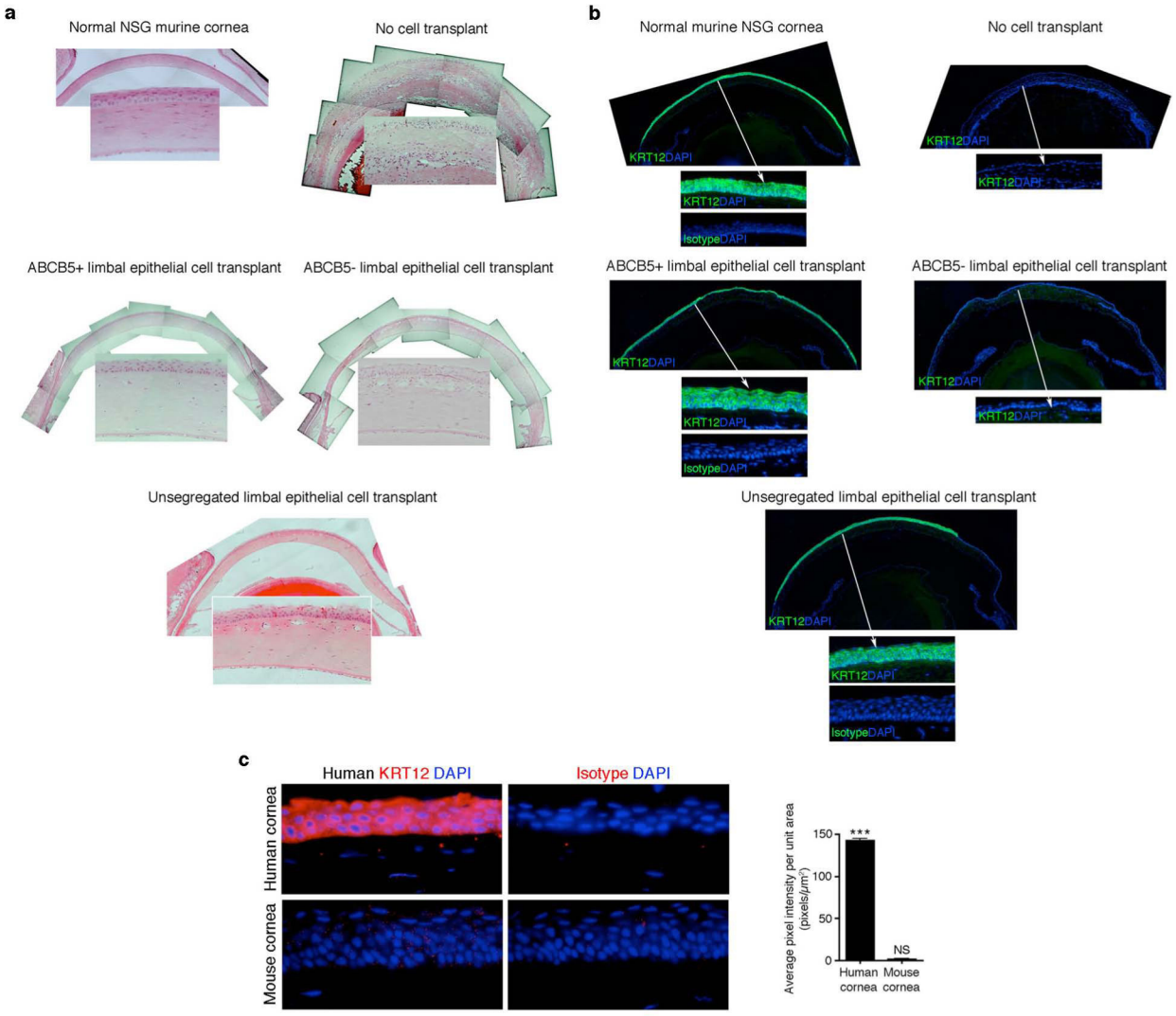

Extended Data Figure 9. Long-term corneal restoration by donor human ABCB5$^+$ cell transplants 13 months after transplantation

a, Representative H&E composite corneal cross-sections of recipient immunodeficient NSG mice 13 months after LSCD induction followed by transplantation of donor fibrin gel grafts containing: (1) no cells (negative control), (2) ABCB5$^+$ cells, (3) ABCB5$^-$ cells, and (4) unsegregated cells. A normal untreated NSG cornea (no LSCD) served as a positive control. The positive control displays the typical stratified corneal epithelium. Mice that received transplants with no cells displayed evidence of conjunctivalization that occurs following a LSC deficiency; that is, unstratified conjunctival epithelium covers the cornea with extensive neovascularization and synechia (anterior segment inflammation is muted in NSG mice due to their immunodeficiency). In contrast, mice that received transplants containing ABCB5$^+$ cells displayed restored stratified epithelium, whereas recipients receiving ABCB5$^-$ cell grafts did not. **b**, Representative immunofluorescent KRT12 staining (green) of corneas derived from NSG mice 13 months after LSCD induction followed by transplantation of donor fibrin gel grafts containing the following human limbal epithelial

NIH-PA Author Manuscript NIH-PA Author Manuscript NIH-PA Author Manuscript

NIH-PA Author Manuscript

NIH-PA Author Manuscript

NIH-PA Author Manuscript

cell subpopulations: (1) no cells (negative control), (2) ABCB5^{+} cells, (3) ABCB5^{-} cells, or (4) unsegregated cells. Normal untreated murine cornea (no LSCD), shown here as a positive control, displayed a high intensity of KRT12 staining. As expected, recipients of grafts containing no cells displayed no KRT12 expression. Mice transplanted with ABCB5^{+} cells exhibited significant KRT12 expression, also enhanced compared to mice transplanted with unsegregated limbal epithelial cells. No KRT12 expression was detected in mice transplanted with ABCB5^{-} cells. The white arrow depicts the area shown at ×40 magnification. Montage images are shown at ×10 magnification. **c**, Representative immunofluorescent KRT12 staining (red) of human and mouse cornea confirms specific antibody reactivity with human KRT12 (top left), and no cross-reactivity with murine Krt12 (bottom left). Isotype control antibody staining is shown for the respective tissues in the right panels. Nuclei are stained with DAPI (blue). Bar graph (bottom) demonstrates aggregate antibody staining data of either human cornea (pixel intensity 142.3 ± 2.4 pixels μm^{-2}, mean ± s.e.m.) or mouse cornea (pixel intensity 1.3 ± 0.7 pixels μm^{-2}, mean ± s.e.m.). Aggregate human KRT12 antibody staining data of either human or mouse cornea was derived from the analyses on $n = 2$ corneas per group. Within a standardized area in (**b**), all corneal epithelial cells were counted in at least $n = 3$ consecutive cross-sections. Data were analysed using the unpaired *t*-test. Error bars show s.e.m. ***$P < 0.001$. NS, not significant.

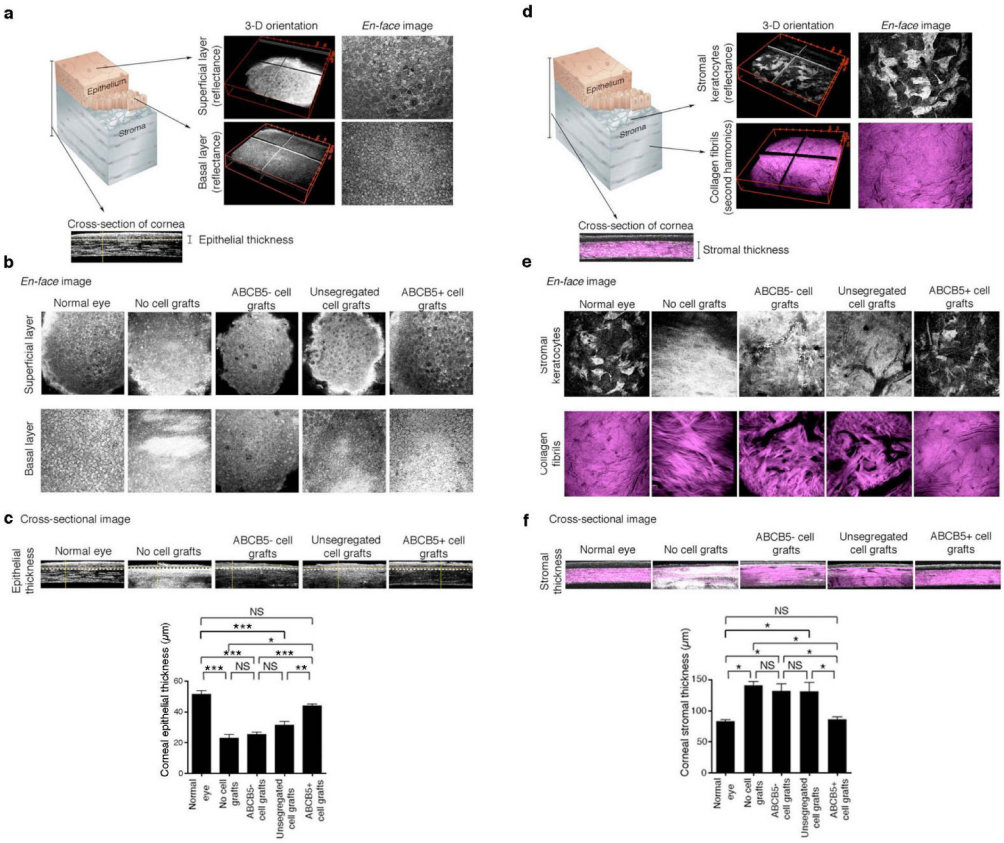

Extended Data Figure 10. Corneal epithelial restoration in 13-month-old human transplants

NIH-PA Author Manuscript

NIH-PA Author Manuscript

NIH-PA Author Manuscript

a–**c**, Corneal epithelial restoration in 13-month-old human transplants examined by reflectance confocal microscopy. **a**, Schematic illustration of the cornea. **b**, **c**, Confocal microscopic reflectance was used to image 400 × 400 μm areas in the central cornea in the normal eye, as well as control and treatment groups. Representative *en face* images of normal corneal epithelial layers depicting superficial squamous and basal cuboidal epithelial cells, and the corresponding cross-sectional image depicting the epithelial layer thickness, are shown in the extreme left panels of **b** and **c**, respectively. Additional panels in **b** and **c** from left to right show, show representative *en face* (**b**) and cross-sectional (**c**) images of recipient NSG mice 13 months after LSCD induction followed by transplantation of donor fibrin gel grafts containing the following human limbal epithelial cell subpopulations: (1) no cells (negative control), (2) $ABCB5^-$ cells, (3) unsegregated cells, or (4) $ABCB5^+$ cells. Normal untreated cornea (no LSCD), shown here as a positive control, displayed a typical stratified epithelium of normal thickness. Mice that received grafts containing no cells displayed no stratified epithelium and a significantly reduced epithelial layer. Mice transplanted with $ABCB5^-$ cells displayed a thin unstratified epithelium that was not significantly different from the negative control group. Mice transplanted with unsegregated limbal cells displayed a mixture of stratified and unstratified epithelium that was significantly thinner compared to normal corneas. In contrast, only mice transplanted with $ABCB5^+$ cells displayed a normal stratified epithelium with superficial squamous and basal cuboidal epithelial cells, and a thickness not only significantly greater than in alternative treatment or untreated control groups, but comparable to normal healthy cornea (no significant difference), as determined by measurements of cross-sectional image data. Epithelial layer thickness measurements were performed in all groups using ImageJ software and cross-sectional reflectance confocal microscopy imaging (4 mice per group, 10 measurements per cornea) through the central region of the cornea. The measurements were performed on mice from two independent experiments. Data were analysed using the one-way ANOVA and Bonferroni multiple comparisons tests. Aggregate results are illustrated in **c**, bottom panel bar graph (mean thickness in micrometres (μm) ± s.e.m.). **d**–**f**, Corneal stromal architecture of 13-month-old human transplants examined by reflectance confocal and second harmonic generation microscopy. **d**, Schematic illustration of the cornea. **e**, **f**, Reflectance confocal and second harmonic generation microscopy was used to image 400 × 400 μm areas in the central stroma of the normal eye, as well as of control and treatment groups. Representative *en face* images of normal cornea (**e**, extreme left panels) show normal stromal keratocytes as determined by confocal reflectance (top) and stromal architecture as determined by second harmonic generation of collagen fibrils (magenta images, bottom). The corresponding cross-sectional image depicting the stroma layer thickness is shown in the extreme left of panel **f**. Additional panels in **e** and **f** from left to right show representative *en face* and cross-sectional images of recipient NSG mice 13 months after LSCD induction followed by transplantation of donor fibrin gel grafts containing the following human limbal epithelial cell subpopulations: (1) no cells (negative control), (2) $ABCB5^-$ cells, (3) unsegregated cells, or (4) $ABCB5^+$ cells. Normal untreated cornea (no LSCD), shown here as a positive control, displayed typical stromal keratocytes and a normal collagen fibril pattern, with normal stromal thickness determined in cross-sectional images. Mice that received grafts containing no cells displayed a high level of reflectance due to inflammation (also compare H&E staining in Extended Data Fig. 9a) and

NIH-PA Author Manuscript

NIH-PA Author Manuscript

NIH-PA Author Manuscript

stromal oedema as shown by increased stromal thickness. In addition, an abnormal collagen fibril pattern was observed, possibly due to deposition of new collagen by infiltrating inflammatory cells. Mice transplanted with $ABCB5^{-}$ cells displayed a high level of reflectance, an abnormal collagen fibril pattern, and stromal oedema that was not significantly different from the negative control group. Mice transplanted with unsegregated limbal cells also displayed increased reflectance, an abnormal collagen fibril pattern, and stromal oedema. In contrast, only mice transplanted with $ABCB5^{+}$ cells displayed a normal pattern of stromal keratocytes and collagen fibrils, and a stromal thickness comparable to normal healthy cornea (no significant difference) and indicative of absent oedema, as determined by measurements of cross-sectional image data. Stromal thickness measurements were performed in all groups using ImageJ software and cross-sectional second harmonic microscopic images of collagen fibrils (4 mice per group, 5 measurements per stroma) through the central region of the stroma. The measurements were performed on mice from two independent experiments. Data were analysed using the one-way ANOVA and Bonferroni multiple comparisons tests. Aggregate results are illustrated in **f**, bottom panel bar graph (mean thickness in μm ± s.e.m.). Error bars show s.e.m. $*P < 0.05$, $**P < 0.01$, $***P < 0.001$. NS, not significant. Magnification in **a**–**f**: ×60.

Supplementary Material

Refer to Web version on PubMed Central for supplementary material.

Acknowledgments

We thank R. Maas for critical reading of the manuscript. We also thank P. Mallen for assistance with graphic illustrations; the Heartland Lions Eye Bank for providing clinical specimens; G. Berg for assistance with mouse colony maintenance; D. Dombkowski, F. Preffer and R. Huang for their assistance with cell sorting and viability studies. This work was supported by National Institutes of Health (NIH)/National Institutes of Neurological Disorders and Stroke grant K08NS051349, VA BLR&D 1I01BX000516 and VA RR&D 1I01RX000989 Merit Review Awards, and a Harvard Stem Cell Institute grant to N.Y.F., NIH/National Cancer Institute grants R01CA113796, R01CA158467 and R01CA138231 to M.H.F., Department of Defense grant PR0332453 to B.R.K., NIH R01EY018624 and P30EY014801 grants to V.L.P., NIH grant R01EY021768 to W.W.K., NIH New Innovator Award DP2OD007483 and a Corley Research Foundation grant to B.A.T., NIH R01CA138231 to G.F.M., Western Pennsylvania Medical Eye Bank Core Grant for Vision Research (EY08098) to K.L.L., and NIH grants R01 EB017274, U01HL100402 and P41EB015903 to C.P.L. F.C.G. is a Howard Hughes Medical Institute Fellow of the Life Sciences Research Foundation.

References

1. Davanger M, Evensen A. Role of the pericorneal papillary structure in renewal of corneal epithelium. Nature. 1971; 229:560–561. [PubMed: 4925352]
2. Cotsarelis G, Cheng SZ, Dong G, Sun TT, Lavker RM. Existence of slow-cycling limbal epithelial basal cells that can be preferentially stimulated to proliferate: implications on epithelial stem cells. Cell. 1989; 57:201–209. [PubMed: 2702690]
3. Majo F, Rochat A, Nicolas M, Jaoude GA, Barrandon Y. Oligopotentstem cells are distributed throughout the mammalian ocular surface. Nature. 2008; 456:250–254. [PubMed: 18830243]
4. Dua HS, Joseph A, Shanmuganathan VA, Jones RE. Stem cell differentiation and the effects of deficiency. Eye (Lond). 2003; 17:877–885. [PubMed: 14631392]
5. Rama P, et al. Limbal stem-cell therapy and long-term corneal regeneration. N Engl J Med. 2010; 363:147–155. [PubMed: 20573916]
6. Frank NY, et al. Regulation of progenitor cell fusion by ABCB5 P-glycoprotein, a novel human ATP-binding cassette transporter. J Biol Chem. 2003; 278:47156–47165. [PubMed: 12960149]

NIH-PA Author Manuscript NIH-PA Author Manuscript NIH-PA Author Manuscript

7. Schatton T, et al. Identification of cells initiating human melanomas. Nature. 2008; 451:345–349. [PubMed: 18202660]
8. Pellegrini G, et al. p63 identifies keratinocyte stem cells. Proc Natl Acad Sci USA. 2001; 98:3156–3161. [PubMed: 11248048]
9. Luo Y, et al. Side population cells from human melanoma tumors reveal diverse mechanisms for chemoresistance. J Invest Dermatol. 2012; 132:2440–2450. [PubMed: 22622430]
10. Wilson BJ, et al. ABCB5 identifies a therapy-refractory tumor cell population in colorectal cancer patients. Cancer Res. 2011; 71:5307–5316. [PubMed: 21652540]
11. Frank NY, et al. ABCB5-mediated doxorubicin transport and chemoresistance in human malignant melanoma. Cancer Res. 2005; 65:4320–4333. [PubMed: 15899824]
12. Lin JY, et al. Genetically determined ABCB5 functionality correlates with pigmentation phenotype and melanoma risk. Biochem Biophys Res Commun. 2013; 436:536–542. [PubMed: 23770371]
13. Notara M, Daniels JT. Biological principals and clinical potentials of limbal epithelial stem cells. Cell Tissue Res. 2008; 331:135–143. [PubMed: 17701219]
14. Rocco A, et al. MDR1-P-glycoprotein behaves as an oncofetal protein that promotes cell survival in gastric cancer cells. Lab Invest. 2012; 92:1407–1418. [PubMed: 22751348]
15. Cheung ST, Cheung PF, Cheng CK, Wong NC, Fan ST. Granulin-epithelin precursor and ATP-dependent binding cassette (ABC)B5 regulate liver cancer cell chemoresistance. Gastroenterology. 2011; 140:344–355. [PubMed: 20682318]
16. Liu P, Jenkins NA, Copeland NG. A highly efficient recombineering-based method for generating conditional knockout mutations. Genome Res. 2003; 13:476–484. [PubMed: 12618378]
17. Rodríguez CI, et al. High-efficiency deleter mice show that FLPe is an alternative to Cre-*loxP*. Nature Genet. 2000; 25:139–140. [PubMed: 10835623]
18. Hutcheson DA, Kardon G. Genetic manipulations reveal dynamic cell and gene functions: Creating a new view of myogenesis. CellCycle. 2009; 8:3675–3678.
19. Lakso M, et al. Efficient *in vivo* manipulation of mouse genomic sequences at the zygote stage. Proc Natl Acad Sci USA. 1996; 93:5860–5865. [PubMed: 8650183]
20. Frank NY, et al. VEGFR-1 expressed by malignant melanoma-initiating cells is required for tumor growth. Cancer Res. 2011; 71:1474–1485. [PubMed: 21212411]
21. Pellegrini G, et al. Location and clonal analysis of stem cells and their differentiated progeny in the human ocular surface. J Cell Biol. 1999; 145:769–782. [PubMed: 10330405]
22. Meyer-Blazejewska EA, et al. Preservation of the limbal stem cell phenotype by appropriate culture techniques. Invest Ophthalmol Vis Sci. 2010; 51:765–774. [PubMed: 19710417]
23. Krulova M, et al. A rapid separation of two distinct populations of mouse corneal epithelial cells with limbal stem cell characteristics by centrifugation on percoll gradient. Invest Ophthalmol Vis Sci. 2008; 49:3903–3908. [PubMed: 18469183]
24. Lathrop KL, Gupta D, Kagemann L, Schuman JS, Sundarraj N. Optical coherence tomography as a rapid, accurate, noncontact method of visualizing the palisades of Vogt. Invest Ophthalmol Vis Sci. 2012; 53:1381–1387. [PubMed: 22266521]
25. Kao WW, et al. Keratin 12-deficient mice have fragile corneal epithelia. Invest Ophthalmol Vis Sci. 1996; 37:2572–2584. [PubMed: 8977471]
26. Pal-Ghosh S, Tadvalkar G, Jurjus RA, Zieske JD, Stepp MA. BALB/c and C57BL6 mouse strains vary in their ability to heal corneal epithelial debridement wounds. Exp Eye Res. 2008; 87:478–486. [PubMed: 18809399]
27. Hutcheon A, Sippel KC, Zieske JD. Examination of the restoration of epithelial barrier function following superficial keratectomy. Exp Eye Res. 2007; 84:32–38. [PubMed: 17067576]
28. Klocke J, et al. Spontaneous bacterial keratitis in CD36 knockout mice. Invest Ophthalmol Vis Sci. 2011; 52:256–263. [PubMed: 20847111]
29. Pellegrini G, et al. The control of epidermal stem cells (holoclones) in the treatment of massive full-thickness burns with autologous keratinocytes cultured on fibrin. Transplantation. 1999; 68:868–879. [PubMed: 10515389]

NIH-PA Author Manuscript

NIH-PA Author Manuscript

NIH-PA Author Manuscript

30. Meyer-Blazejewska EA, et al. From hair to cornea: toward the therapeutic use of hair follicle-derived stem cells in the treatment of limbal stem cell deficiency. Stem Cells. 2011; 29:57–66. [PubMed: 20957740]

31. Veilleux I, Spencer JA, Biss DP, Côté D, Lin CP. *In vivo* cell tracking with video rate multimodality laser scanning microscopy. IEEE J Sel Top Quant Electron. 2008; 14:10–18.

32. Wang K, et al. Three-color femtosecond source for simultaneous excitation of three fluorescent proteins in two-photon fluorescence microscopy. Biomed Opt Express. 2012; 3:1972–1977. [PubMed: 23024893]

NIH-PA Author Manuscript
NIH-PA Author Manuscript
NIH-PA Author Manuscript

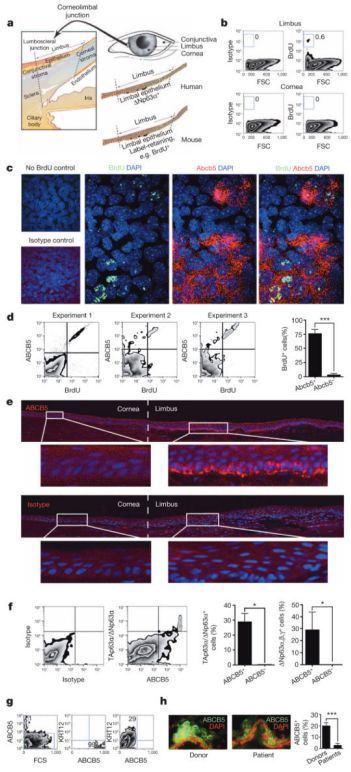

Figure 1. ABCB5 marks LSCs

a, Cornea and LSC niche. **b**, BrdU detection (8-week chase). **c**, **d**, Immunofluorescence (×60 magnification) (**c**) and flow cytometric staining (gating based on control-staining) (**d**) for Abcb5/BrdU co-expression in mouse limbus. DAPI, 4′,6-diamidino-2-phenylindole. Abcb5 and BrdU co-expression data in **d** represent analyses of $n = 4$ mice per group (mean ± standard error of the mean (s.e.m.)). The experiment was performed three times. Data were analysed using the unpaired *t*-test, $P < 0.001$. **e**, ABCB5 positivity in human limbus (palisades of Vogt, ×20 magnification), with negativity in central cornea. **f**, ABCB5/p63α co-expression in human limbus. Quantitative analysis of ABCB5 monoclonal antibody and ΔNp63α/TAp63α epitope-binding antibody co-expression was performed using limbal epithelial cells from $n = 4$ eyes. The experiment was performed twice. Data were analysed using the unpaired *t*-test. Data are shown as mean ± s.e.m., $P < 0.05$. The quantitative analysis of ABCB5 monoclonal antibody and ΔNp63α,β,γ epitope binding antibody co-expression was performed using limbal epithelial cells from $n = 4$ eyes. The experiment was performed twice. Data were analysed using the Mann–Whitney test. Data are shown as mean ± s.e.m., $P < 0.05$. **g**, ABCB5/KRT12 co-expression. FSC, forward scatter. **h**, ABCB5 in LSCD patients (×20 magnification). Bar graph shows per cent $ABCB5^+$ cells in control donors versus LSCD patients. Quantitative analysis of ABCB5 expression in $n = 2$ control and $n = 2$ LSCD specimens was performed using $n = 8$ sections per patient/control. All epithelial cells were counted in each section. A total of 2,031 and 2,051 epithelial cells were counted in patient 1 and donor 1, respectively. A total of 563 and 2,662 epithelial cells were counted in patient 2 and donor 2, respectively. Data were analysed using the unpaired *t*-test. Error bars indicate s.e.m. $*P < 0.05$, $***P < 0.001$.

NIH-PA Author Manuscript

NIH-PA Author Manuscript

NIH-PA Author Manuscript

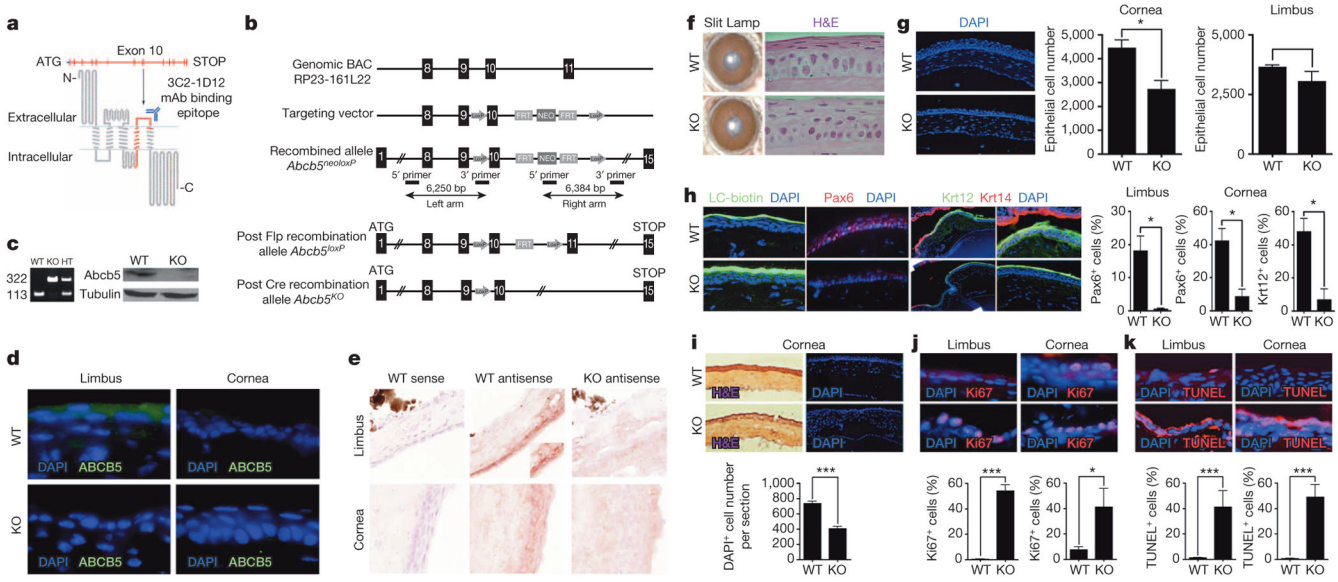

Figure 2. ABCB5 regulates corneal development and repair

a, *Abcb5* locus and protein topology (transmembrane protein topology with a hidden Markov model (TMHMM), knockout deletion in red). mAb, monoclonal antibody. **b**, *Abcb5* knockout strategy. BAC, bacterial artificial chromosome. **c**, PCR and western blot in wild-type (WT) versus knockout (KO) mice. HT, heterozygous. **d**, **e**, Abcb5 immunofluorescence staining (**d**) and *in situ* hybridization (**e**) of wild-type and knockout limbus and cornea (×20 magnification). **f**–**h**, Slit lamp and haematoxylin and eosin (H&E; ×40 magnification) (**f**), cellularity (**g**) and LC-biotin diffusion and protein expression (**h**) analyses. **i**, Analysis of wild-type and knockout corneas following debridement wounding. **j**, **k**, Ki67 immunofluorescence (**j**) and TdT-mediated dUTP nick end labelling (TUNEL) (**k**) staining. **g**–**k**, ×20 magnification. **g**, The numbers of viable epithelial cells in *Abcb5* knockout versus *Abcb5* wild-type murine central cornea were derived from the analysis of $n = 8$ mice per group (left bar graph). The experiment was performed four times. Data were analysed using the unpaired *t*-test. Data are shown as mean ± s.e.m., $P < 0.05$. In the right bar graph, the numbers of viable epithelial cells in *Abcb5* knockout versus *Abcb5* wild-type murine limbus were derived from the analysis of $n = 6$ mice per group. The experiment was performed three times. Data were analysed using the unpaired *t*-test. Data are shown as mean ± s.e.m., P = not significant. **h**, Quantitative analyses of Pax6 expression in limbus and cornea of *Abcb5* knockout versus *Abcb5* wild-type mice were performed using $n = 3$ mice per group. The experiment was performed three times. Ten thousand cells per experiment were counted for each group. Data were analysed using the unpaired *t*-test. Data are shown as mean ± s.e.m., $P < 0.05$. Quantitative analyses of Krt12 expression in cornea were performed using $n = 2$ mice per group. The experiment was performed twice. Ten thousand cells per experiment were counted for each group. Data were analysed using the unpaired *t*-test. Data are shown as mean ± s.e.m., $P < 0.05$. **i**, The numbers of $DAPI^+$ cells per section in *Abcb5* wild-type versus *Abcb5* knockout mice (mean ± s.e.m.) were derived from $n = 6$ mice per group. The experiment was performed twice. Within the standardized area (shown in Extended Data Fig. 4f), all corneal epithelial cells were counted in at least $n = 3$ consecutive

NIH-PA Author Manuscript

NIH-PA Author Manuscript

NIH-PA Author Manuscript

composite cross-sections. Data were analysed using the unpaired *t*-test, $P < 0.001$. **j**, The percentages of $Ki67^+$ epithelial cells in limbus and cornea of *Abcb5* knockout versus *Abcb5* wild-type mice (mean ± s.e.m.) were determined using $n = 4$ mice per group. The experiment was performed twice. Within a standardized area, all limbal epithelial cells were counted in at least $n = 3$ consecutive cross-sections. Data were analysed using the unpaired *t*-test, $P < 0.001$ for limbus and $P < 0.05$ for cornea. **k**, The percentages of $TUNEL^+$ epithelial cells in limbus or cornea of *Abcb5* knockout versus *Abcb5* wild-type mice (mean ± s.e.m.) were determined using $n = 4$ mice per group. The experiment was performed twice. Within a standardized area, all limbal epithelial cells were counted in at least $n = 3$ consecutive cross-sections. Data were analysed using the unpaired *t*-test, $P < 0.001$ for limbus and $P < 0.001$ for cornea. Error bars indicate s.e.m. $^*P < 0.05$, $^{***}P < 0.001$. NS, not significant.

NIH-PA Author Manuscript

NIH-PA Author Manuscript

NIH-PA Author Manuscript

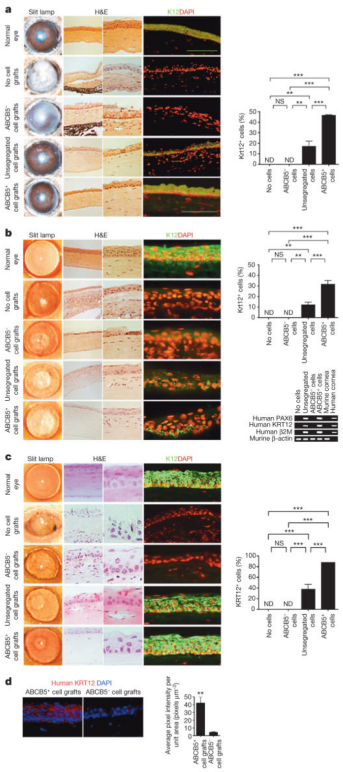

Figure 3. Regenerative role of ABCB5$^+$ LSCs

a, **b**, Murine syngeneic grafts (**a**) and 5-week (**b**) or 13-month (**c**) human xenografts to LSCD-induced mice. Grafts contained either no donor cells (row 2), ABCB5$^-$ cells (row 3), unsegregated cells (row 4), or ABCB5$^+$ cells (row 5). **a**–**c**, Untreated C57BL/6 (**a**) and NSG (**b**, **c**) corneas (without LSCD) are shown in row 1. **b**, Bottom right, RT–PCR detection of human donor cells. **d**, Human KRT12$^+$ cells (red) in recipient corneas of ABCB5$^+$ human grafts at 13 months. Magnification: columns 2 and 4: ×20; column 3: ×40. Scale bars: 100 μm. The transplantation experiments shown in **a** and **b** were performed in $n = 5$ mice per group. The experiment was performed twice. For KRT12 expression analyses, all corneal epithelial cells within a standardized area (Extended Data Fig. 8b) were counted in at least $n = 3$ consecutive cross-sections from $n = 4$ replicate mice per group. Data were analysed using the one-way ANOVA and Bonferroni multiple comparisons tests. Data are shown as mean ± s.e.m. **c**, The transplantation experiments were performed in $n = 5$ mice per group. The experiment was performed twice. For KRT12 expression analyses, all corneal epithelial cells within a standardized area (Extended Data Fig. 9b) were counted in at least $n = 3$ consecutive cross-sections from $n = 4$ replicate mice per group. Data were analysed using the one-way ANOVA and Bonferroni multiple comparisons tests. Data are shown as mean ± s.e.m. **d**, Human KRT12 expression was analysed in $n = 4$ mice per group. Within a standardized area (Extended Data Fig. 9b), all corneal epithelial cells were counted in at least $n = 3$ consecutive cross-sections. Data were analysed using the unpaired *t*-test. Data are shown as mean ± s.e.m. Error bars indicate s.e.m. $^{**}P < 0.01$, $^{***}P < 0.001$. ND, not detected; NS, not significant.